Published for SISSA by Springer

Received: December 17, 2024
Revised: March 8, 2025
Accepted: April 23, 2025
Published: May 22, 2025

Amplitude analysis and branching fraction measurement of the Cabibbo-favored decay $D^+ \to K^-\pi^+\pi^+\pi^0$

The BESIII collaboration

E-mail: besiii-publications@ihep.ac.cn

Abstract: An amplitude analysis of the Cabibbo-favored decay $D^+ \to K^-\pi^+\pi^+\pi^0$ is performed, using 7.93 fb^{-1} of e^+e^- collision data collected with the BESIII detector at the center-of-mass energy of 3.773 GeV. The branching fractions of the intermediate processes are measured, with the dominant contribution $D^+ \to \bar{K}^*(892)^0\rho(770)^+$ observed to have a branching fraction of $(4.35 \pm 0.07_{\rm stat.} \pm 0.17_{\rm syst.})\%$. With the detection efficiency derived from the amplitude analysis, the absolute branching fraction of $D^+ \to K^-\pi^+\pi^+\pi^0$ is measured to be $(6.35 \pm 0.04_{\rm stat.} \pm 0.07_{\rm syst.})\%$.

Keywords: Branching fraction, Charm Physics, e^+-e^- Experiments

ArXiv ePrint: 2412.11040

https://doi.org/10.1007/JHEP05(2025)195

JHEP05(2025)195

Contents

1 Introduction

The Cabibbo-favored (CF) decay $D^+ \to K^-\pi^+\pi^+\pi^0$ serves as one of golden "tag mode" (the other is $D^+ \to K^-\pi^+\pi^+$) for measurements related to the D meson [1–3], given its large branching fraction (BF) and low background contamination. A first measurement of the BF and an amplitude analysis of $D^+ \to K^-\pi^+\pi^+\pi^0$ were performed by the Mark III collaboration [4] using a limited data sample. The CLEO collaboration subsequently improved the precision of the BF measurement [5], but did not report any study of the intermediate resonances.

Recently, the doubly-Cabibbo-suppressed (DCS) decay $D^+ \to K^+\pi^+\pi^-\pi^0$ was observed for the first time [3] and its BF was measured to be $(1.13 \pm 0.08_{\rm stat.} \pm 0.03_{\rm syst.}) \times 10^{-3}$. After combining the averaged value of BF for its counterpart CF decay $D^+ \to K^-\pi^+\pi^+\pi^0$ [6], the ratio of $\frac{\mathcal{B}(D^+\to K^+\pi^+\pi^-\pi^0)}{\mathcal{B}(D^+\to K^-\pi^+\pi^+\pi^0)}$ is determined to be $(1.81 \pm 0.15)\%$ corresponding to $(6.28 \pm 0.52)\tan^4\theta_C$, where θ_C is the Cabibbo mixing angle. This ratio is significantly larger than the naive expectation for the DCS rate relative to its CF counterpart decay (0.21–0.58)% [7–9], which implies that some unknown effects are contributing to either or both of the two

JHEP05(2025)195

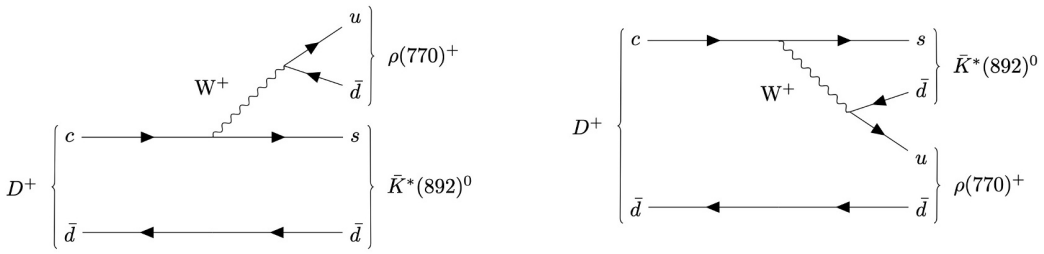

Figure 1. The Feynman diagrams of $D^+ \to \bar{K}^*(892)^0\rho(770)^+$.

decays and motivates gaining an improved understanding of the resonance structure of $D^+ \to K^-\pi^+\pi^+\pi^0$.

Comparing to the case of many well-studied three-body decays [10–13], an amplitude analysis of $D^+ \to K^-\pi^+\pi^+\pi^0$ can provide further insights into more complicated dynamics and substructures in the D-meson decays to two vector mesons $D \to VV$, which have attracted a great deal of attention in both theory and experiment [14–21], but where there is limited available experimental information. Figure 1 shows the leading Feynman diagrams of the two vector mesons decay $D^+ \to \bar{K}^*(892)^0\rho(770)^+$. Furthermore, measurements of the D meson decays to axial-vector and pseudoscalar mesons $D \to AP$, such as $D^+ \to \bar{K}_1(1270)^0\pi^+$ and $D^+ \to \bar{K}_1(1400)^0\pi^+$, are also beneficial for the understanding of the mixing angle between axial-vectors θ_{K_1} [22, 23].

In this paper we present the amplitude analysis and BF measurement of the decay $D^+ \to K^-\pi^+\pi^+\pi^0$, utilizing 7.93 fb^{-1} of e^+e^- collision data collected at a center-of-mass energy $\sqrt{s} = 3.773$ GeV by the BESIII detector at BEPCII [24, 25]. A double tag (DT) method is employed by reconstructing D^+D^- from $D^+ \to K^-\pi^+\pi^+\pi^0$ and $D^- \to K^+\pi^-\pi^-$, respectively. Charged-conjugate modes and exchange symmetry of two identical π^+ are always implied throughout.

2 Detector and data

The BESIII detector [26] records symmetric e^+e^- collisions provided by the BEPCII storage ring [27] in the center-of-mass energy range from 1.85 to 4.95 GeV, with a peak luminosity of 1.1×10^{33} cm^{-2}s^{-1} achieved at $\sqrt{s} = 3.773$ GeV. BESIII has collected large data samples in this energy region [28–30]. The cylindrical core of the BESIII detector covers 93% of the full solid angle and consists of a helium-based multilayer drift chamber (MDC), a plastic scintillator time-of-flight system (TOF), and a CsI(Tl) electromagnetic calorimeter (EMC), which are all enclosed in a superconducting solenoidal magnet providing a 1.0 T magnetic field. The solenoid is supported by an octagonal flux-return yoke with resistive plate counter muon identification modules interleaved with steel. The charged-particle momentum resolution at 1 GeV/c is 0.5%, and the ionization energy loss (dE/dx) resolution in MDC is 6% for electrons from Bhabha scattering. The EMC measures photon energies with a resolution of 2.5% (5%) at 1 GeV in the barrel (end-cap) region. The time resolution in the TOF barrel region is 68 ps, while that in the end-cap region was 110 ps. The end-cap TOF system

was upgraded in 2015 using multigap resistive plate chamber technology, providing a time resolution of 60 ps, which benefits 63% of the data used in this analysis [31–33].

Monte Carlo (MC) simulated data samples produced with a GEANT4-based [34] software package, which includes the geometric description of the BESIII detector and the detector response, are used to determine detection efficiencies and estimate backgrounds. The simulation models the beam-energy spread and initial-state radiation (ISR) in the e^+e^- annihilations with the generator KKMC [35, 36]. The inclusive MC sample includes the production of $D\bar{D}$ pairs which contains quantum coherence for the neutral D channels, the non-$D\bar{D}$ decays of the $\psi(3770)$, the ISR production of the J/ψ and $\psi(3686)$ states, and the continuum processes incorporated in KKMC [35, 36]. All particle decays are modeled with EVTGEN [37, 38] using BFs either taken from the Particle Data Group [6], when available, or otherwise estimated with LUNDCHARM [39, 40]. Final-state radiation from charged final-state particles is incorporated using the PHOTOS package [41].

In this work, two sets of MC samples are used: the phase space (PHSP) MC sample and the signal MC sample. For the tag process $D^- \to K^+\pi^+\pi^-$, both sets of MC samples are simulated using the model derived from the amplitude analysis reported in ref. [12]. In the PHSP MC sample the signal process $D^+ \to K^-\pi^+\pi^+\pi^0$ is generated with a uniform distribution in PHSP in order to allow the calculation of the normalization factor of the probability density function (PDF) used in the amplitude analysis. In the signal MC sample, the signal process is generated based on the results of the amplitude analysis and is used to estimate the detection efficiencies.

3 Event selection

Charged tracks detected in the MDC are required to be within a polar angle (θ) range of $|\cos\theta| < 0.93$, where θ is defined with respect to the z-axis, which is the symmetry axis of the MDC. For charged tracks, the distance of closest approach to the interaction point (IP) must be less than 10 cm along the z-axis, $|V_z|$, and less than 1 cm in the transverse plane, $|V_{xy}|$.

Photon candidates are identified using isolated showers in the EMC. The deposited energy of each shower must be more than 25 MeV in the barrel region ($|\cos\theta| < 0.80$) and more than 50 MeV in the end-cap region ($0.86 < |\cos\theta| < 0.92$). To exclude showers that originate from charged tracks, the angle subtended by the EMC shower and the position of the closest charged track at the EMC must be greater than 10 degrees as measured from the IP. To suppress electronic noise and showers unrelated to the event, the difference between the EMC time and the event start time is required to be within [0, 700] ns.

Particle identification (PID) for charged tracks combines measurements of the $\mathrm{d}E/\mathrm{d}x$ and the flight time in the TOF to form likelihoods $\mathcal{L}(h)$ ($h = K, \pi$) for each hadron h hypothesis. Charged kaons and pions are identified by comparing the likelihoods, $\mathcal{L}(K) > \mathcal{L}(\pi)$ and $\mathcal{L}(\pi) > \mathcal{L}(K)$, respectively.

The π^0 candidates are formed from the photon pairs with invariant masses in a range of $[0.115, 0.150]\,\mathrm{GeV}/c^2$, which is about three times the mass resolution. Moreover, in order to achieve an adequate resolution, at least one of the two photons is required to be detected in the barrel EMC. A one-constraint kinematic fit that constrains the $\gamma\gamma$ invariant mass to the

JHEP05(2025)195

known π^0 mass [6] is performed to improve the mass resolution. The χ^2 of the kinematic fit is required to be less than 30.

The D^+D^- pairs are reconstructed from $D^+ \to K^-\pi^+\pi^+\pi^0$ and $D^- \to K^+\pi^-\pi^-$, respectively. To distinguish the D^+D^- mesons from the backgrounds, the beam-constrained mass ($M_{\rm BC}$) and the energy difference (ΔE) are used to identify the signal D^+D^- pair:

$$\begin{aligned} M_{\rm BC} &= \sqrt{E^2_{\rm beam} - |\vec{p}_D|^2}, \\ \Delta E &= E_D - E_{\rm beam}, \end{aligned} \tag{3.1}$$

where $\vec{p}_D$ and E_D are the total reconstructed momentum and energy of the D candidate, and $E_{\rm beam}$ is the beam energy. The D signal manifest itself as a peak around the known D mass [6] in the $M_{\rm BC}$ distribution and as a peak around zero in the ΔE distribution. If multiple DT candidates are present in an event, the one with the smallest quadratic sum of ΔE from the signal and tag sides ($\Delta E^2_{\rm sig} + \Delta E^2_{\rm tag}$) is selected for further analysis.

4 Amplitude analysis

4.1 Further selection criteria

To increase the signal purity for the amplitude analysis, the requirement of $-0.062 < \Delta E < 0.034$ ($-0.025 < \Delta E < 0.025$) GeV for $D^+ \to K^-\pi^+\pi^+\pi^0$ ($D^- \to K^+\pi^-\pi^-$) is applied. To suppress background from $D^0 \to K^-\pi^+\pi^+\pi^-$, $\bar{D}^0 \to K^+\pi^-\pi^0$ events in the $D^+ \to K^-\pi^+\pi^+\pi^0$, $D^- \to K^+\pi^-\pi^-$ sample, where the π^0 from the $\bar{D}^0$ decay and the π^- from the D^0 decay are interchanged, we reconstruct the wrong beam-constrained mass ($M^{\rm W}_{\rm BC}$) and the wrong energy difference ($\Delta E^{\rm W}$) according to the $D^0\bar{D}^0$ decay mode hypothesis. For multiple misidentified candidates, we use the minimum quadratic sum of $\Delta E^{\rm W}$ to select the "best background" event. The $D^0\bar{D}^0$ backgrounds form a peak around the known D^0 mass [6] while the distribution for signal is flat. Events satisfying $1.863 < M^{\rm W}_{\rm BC} < 1.867\,{\rm GeV}/c^2$ for both tag and signal sides are rejected.

A six-constraint kinematic fit is performed, in which the four-momenta of the final-state particles are constrained to the initial four-momenta of the e^+e^- system and the reconstructed masses of D^+ and π^0 are constrained to their known values [6]. The events with $\chi^2 < 100$ are retained, and the modified four-momenta of the final state particles from the kinematic fit are used to perform the amplitude analysis.

After applying all of the aforementioned criteria, the signal yields are extracted from an unbinned two-dimensional (2D) maximum likelihood fit to the distribution of $M^{\rm sig}_{\rm BC}$ versus $M^{\rm tag}_{\rm BC}$ (see appendix A for details). The fit results are depicted in figure 2. A total of 26,709 events with a purity ($P_{\mathcal{S}}$) of $(98.4 \pm 0.1)\%$ in both the $M^{\rm sig}_{\rm BC}$ and $M^{\rm tag}_{\rm BC}$ signal region of [1.863, 1.879] GeV/c^2 are retained for the subsequent amplitude analysis.

4.2 Fit method

An unbinned maximum-likelihood fit is used in the amplitude analysis of $D^+ \to K^-\pi^+\pi^+\pi^0$. The likelihood function $\mathcal{L}$ is constructed with the signal and background PDFs, which depend on the momenta of the four final-state particles. Given the high purity of the signal events,

JHEP05(2025)195

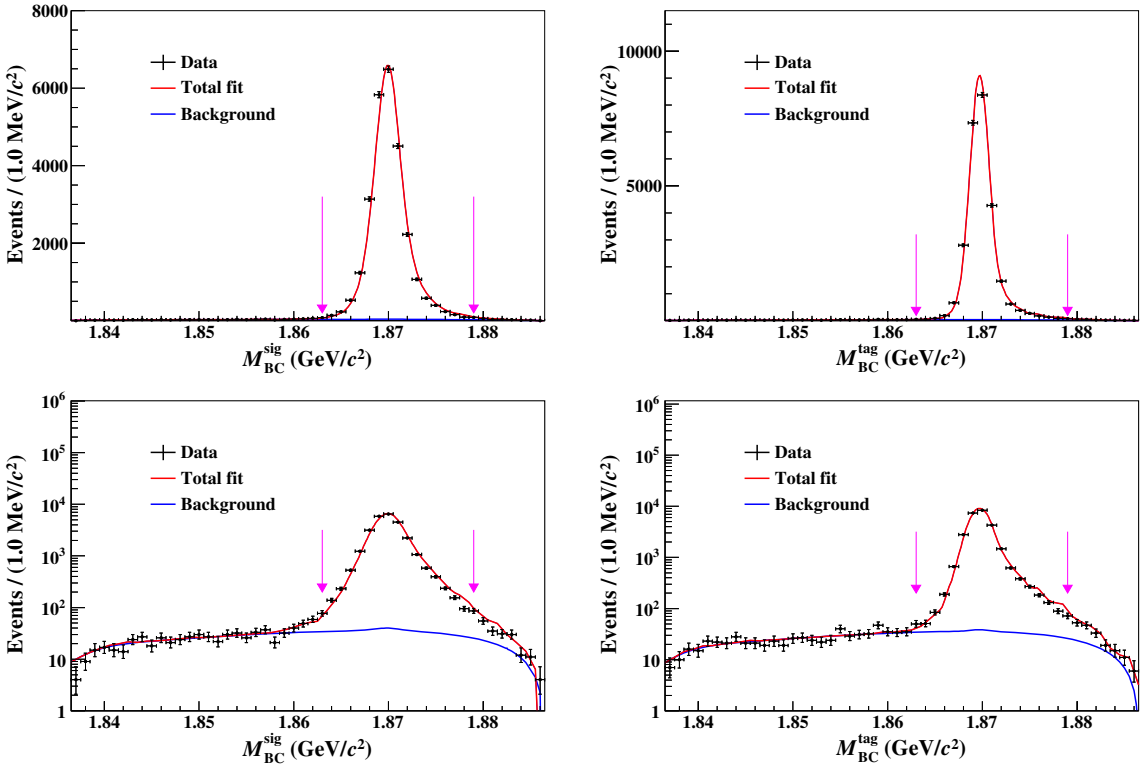

Figure 2. Projections on the $M_{\rm BC}$ distributions of the 2D fit described in the text for the signal (left) and tag (right) sides. The distribution corresponding to the Y-axis logarithmic coordinates is listed in the following two figures. The arrows indicated the boundaries of the selected signal region.

the log-likelihood function is constructed by summing all signal candidates and subtracting the MC-simulated backgrounds:

$$\ln\ \mathcal{L} = \sum_{k_{\rm data}=1}^{N_{\rm data}} \ln\ f_{\rm data}(p^{k_{\rm data}}) - \sum_{k_{\rm bkg}=1}^{N_{\rm bkg}} w_{\rm bkg} \ln\ f_{\rm bkg}(p^{k_{\rm bkg}})\,, \tag{4.1}$$

where $k_{\rm data}$ and $N_{\rm data}$ represent the index of the $k^{\rm th}$ event and the number of the selected signal candidates, respectively. The notation $p^{k_{\rm data}}$ is used to describe the four-momenta of the final-state particles for the $k^{\rm th}$ data candidate, and $f_{\rm data}$ represents the PDF of the data candidate. The symbols with the subscript "bkg" represent the corresponding parameters associated with the MC-simulated backgrounds. Furthermore, $w_{\rm bkg}$ is the weight of MC-simulated backgrounds that is determined by $N_{\rm data} \times (1 - P_{\mathcal{S}})/N_{\rm bkg}$, where $P_{\mathcal{S}}$ is the signal purity discussed in section 4.1.

The PDF for the data candidates and MC-simulated backgrounds are both given by

$$f(p) = \frac{\epsilon(p)\,|\mathcal{M}(p)|^2\,R_4}{\int \epsilon(p)\,|\mathcal{M}(p)|^2\,R_4\,{\rm d}p}\,, \tag{4.2}$$

where $\epsilon(p)$ is the detection efficiency parameterized in terms of the four-momenta p, and R_4 is the PHSP factor for four-body decays. The total amplitude $\mathcal{M}(p)$ is modeled with

JHEP05(2025)195

the isobar model, which is the coherent sum of the individual amplitudes of intermediate processes and is given by $\mathcal{M}(p) = \sum \rho_n e^{i\phi_n} \mathcal{A}_n(p)$, where the magnitude ρ_n and phase ϕ_n are the free parameters to be determined by the fit. For the amplitude of D^- decays, we define the CP conjugate phase space $\bar{p}$ which is transformed to p by the interchange of final state charges and the reversal of three-momenta, and assume CP conservation in the $D^{\pm}$ decay. Then we get $\mathcal{M}_{D^-}(p) = \sum \rho_n e^{i\phi_n} \bar{\mathcal{A}}_n(p) = \sum \rho_n e^{i\phi_n} \mathcal{A}_n(\bar{p})$. The amplitude of the n^{th} intermediate process ($\mathcal{A}_n(p)$) is given by

$$\mathcal{A}_n(p) = P_n^1 P_n^2 S_n F_n^1 F_n^2 F_n^3 \,, \tag{4.3}$$

where the indices 1, 2 and 3 correspond to the two subsequent intermediate resonances and the D^+ meson, respectively. Here, F_n is the Blatt-Weisskopf barrier (section 4.2.1), P_n is the propagator of the intermediate resonance (section 4.2.2), and S_n is the spin factor constructed with the covariant tensor formalism [43] (section 4.2.3). The normalization integral is realized by a signal MC integration to account the resolution on the phase space and width of the narrower resonances,

$$\int \epsilon(p)|\mathcal{M}(p)|^2 R_4 \, \mathrm{d}p \approx \frac{1}{N_{\text{MC}}} \sum_{k_{\text{MC}}}^{N_{\text{MC}}} \frac{|\mathcal{M}(p^{k_{\text{MC}}})|^2}{|\mathcal{M}^g(p^{k_{\text{MC}}})|^2} \,, \tag{4.4}$$

where k_{MC} is the index of the k^{th} event of the signal MC sample, and N_{MC} is the number of the selected signal MC events. The symbol $\mathcal{M}^g(p)$ denotes the PDF used to generate the signal MC sample in the MC integration.

To account for the bias caused by differences in tracking, PID efficiencies, and π^0 reconstruction between data and MC simulation, each signal MC event is weighted with a ratio, $\gamma_\epsilon(p)$, which is calculated as

$$\gamma_\epsilon(p) = \prod_j \frac{\epsilon_{j,\text{data}}(p)}{\epsilon_{j,\text{MC}}(p)}, \tag{4.5}$$

where j denotes the four final-state particles, $\epsilon_{j,\text{data}}(p)$ and $\epsilon_{j,\text{MC}}(p)$ are the tracking, PID and π^0 reconstruction efficiencies as a function of the momentum of the final-state particles for data and MC simulation, respectively. Then the MC integration is determined by

$$\int \epsilon(p)|\mathcal{M}(p)|^2 R_4 \, \mathrm{d}p \approx \frac{1}{N_{\text{MC}}} \sum_{k_{\text{MC}}}^{N_{\text{MC}}} \frac{|\mathcal{M}(p^{k_{\text{MC}}})|^2 \gamma_\epsilon(p^{k_{\text{MC}}})}{|\mathcal{M}^g(p^{k_{\text{MC}}})|^2} \,. \tag{4.6}$$

4.2.1 Blatt-Weisskopf barrier factors

For the process $a \to bc$, the Blatt-Weisskopf barrier factors [44], $X_L(q)$, are parameterized as a function of the angular momentum L and the momenta q of the final-state particle b or c in the rest system of a. They are taken as

$$\begin{aligned} X_{L=0}(q) &= 1, \\ X_{L=1}(q) &= \sqrt{\frac{z_0^2+1}{z^2+1}}, \\ X_{L=2}(q) &= \sqrt{\frac{z_0^4+3z_0^2+9}{z^4+3z^2+9}}, \end{aligned} \tag{4.7}$$

JHEP05(2025)195

where $z = qR_r$, $z_0 = q_0 R_r$ and the effective radius, R_r, of the barrier is fixed to $3.0\,\mathrm{GeV}^{-1}$ for the intermediate resonances and $5.0\,\mathrm{GeV}^{-1}$ for the D^+ meson. The momentum q is given by

$$q = \sqrt{\frac{(s_a + s_b - s_c)^2}{4s_a} - s_b}\,, \tag{4.8}$$

where the value of q_0 is that of q when s_a takes squared of the rest mass of particle a, and $s_a(s_b, s_c)$ denotes the squared invariant-mass of the system consisting of $a(b, c)$.

4.2.2 Propagator

The intermediate resonances $\bar{K}^*(892)^0$, $\bar{K}(1460)^0$, and $\bar{K}^*(1680)^0$ are parameterized with the relativistic Breit-Wigner (RBW) function,

$$P(m) = \frac{1}{m_0^2 - m^2 - im_0\Gamma(m)}\,,\ \Gamma(m) = \Gamma_0 \left(\frac{q}{q_0}\right)^{2L+1} \left(\frac{m_0}{m}\right) X_L^2(q)\,, \tag{4.9}$$

where m is the invariant mass of the decay products, m_0 and Γ_0 are the mass and width of the intermediate resonance that are fixed to their known values [6]. The energy-dependent width is denoted by $\Gamma(m)$.

The decay of the $\bar{K}_1(1270)^0/\bar{K}_1(1400)^0 \to K^-\pi^+\pi^0$ proceeds through a quasi-three-body process, with a complex energy-dependent width that lacks a general analytic expression. The corresponding values are obtained through an iterative method of integrating the squared transition amplitude over the three-body PHSP [45].

The electromagnetic form factor for spin-1 ρ-type resonances is characterized by the Gounaris-Sakurai (GS) function [46]. This function incorporates the finite width of the $\rho(770)$ resonance and serves as a modified version of the RBW lineshape, represented as

$$P_{\mathrm{GS}}(m) = \frac{1 + \mathcal{C}_{\mathrm{GS}}\frac{\Gamma_0}{m_0}}{m_0^2 - m^2 + f(m) - im_0\Gamma(m)}\,. \tag{4.10}$$

The normalization condition at $P_{\mathrm{GS}}(0)$ fixes the parameter $\mathcal{C}_{\mathrm{GS}} = f(0)/(\Gamma_0 m_0)$. It is found to be

$$\mathcal{C}_{\mathrm{GS}} = \frac{3m_\pi^2}{\pi q_0^2}\ln\left(\frac{m_0 + 2q_0}{2m_\pi}\right) + \frac{m_0}{2\pi q_0} - \frac{m_\pi^2 m_0}{\pi q_0^3}\,, \tag{4.11}$$

where m_π is the known π mass [6], . The function $f(m)$ is given by

$$f(m) = \Gamma_0 \frac{m_0^2}{q_0^3}\left[q^2(h(m) - h(m_0)) + (m_0^2 - m^2)q_0^2\,\frac{dh(m)}{d(m^2)}\bigg|_{m_0^2}\right]\,, \tag{4.12}$$

where

$$h(m) = \frac{2q}{\pi m}\ln\left(\frac{m + 2q}{2m_\pi}\right)\,. \tag{4.13}$$

The $K\pi$ S-wave is modeled by the LASS parameterization [47], which is described by a $K_0^*(1430)$ Breit-Wigner together with an effective range non-resonant component with a phase shift. It is given by

$$A(m) = F\sin\delta_F e^{i\delta_F} + R\sin\delta_R e^{i\delta_R} e^{i2\delta_F}\,, \tag{4.14}$$

JHEP05(2025)195

$M_{K_0^*(1430)}(\mathrm{GeV}/c^2)$	1.441 ± 0.002
$\Gamma(\mathrm{GeV})$	0.193 ± 0.004
F	0.96 ± 0.07
ϕ_F (°)	0.1 ± 0.3
R	1(fixed)
ϕ_R (°)	-109.7 ± 2.6
a $(\mathrm{GeV}/c)^{-1}$	0.113 ± 0.006
r $(\mathrm{GeV}/c)^{-1}$	-33.8 ± 1.8

Table 1. The $K\pi$ S-wave parameters are obtained from the amplitude analysis of $D^0 \to K^0_S\pi^+\pi^-$ in the BaBar and Belle experiments [48]. The uncertainties are the combined statistical and systematic uncertainties.

with

$$\begin{aligned}\delta_F &= \phi_F + \cot^{-1}\left[\frac{1}{aq} + \frac{rq}{2}\right],\\ \delta_R &= \phi_R + \tan^{-1}\left[\frac{M_{K_0^*(1430)}\Gamma(m_{K\pi})}{M^2_{K_0^*(1430)} - m^2_{K\pi}}\right].\end{aligned} \tag{4.15}$$

The parameters F, ϕ_F (R and ϕ_R) are the amplitudes and phases of the non-resonant (resonant) component, respectively. The parameters a and r are the scattering length and effective interaction length, respectively. The parameters $M_{K_0^*(1430)}$ and $m_{K\pi}$ are the defined $K_0^*(1430)$ mass and the invariant mass of the $K\pi$ system, respectively. We fix these parameters $(M_{K_0^*(1430)}, \Gamma, F, \phi_F, R, \phi_R, a, r)$ to the results obtained from the amplitude analysis of a sample of $D^0 \to K^0_S\pi^+\pi^-$ decays by the BaBar and Belle experiments [48]. The values of these parameters are summarized in table 1.

4.2.3 Spin factors

Due to the limited size of the PHSP, we only consider intermediate resonances with $J = 0,\ 1,$ and 2. In the process $a \to bc$, we focus exclusively on systems with orbital angular momentum $L = 0,\ 1,$ and 2. The momenta of the particles a, b, and c in the $a \to bc$ process are represented as p_a, p_b, and p_c, respectively. The spin-projection operators [43] are defined as

$$\begin{aligned}P^{(0)}(a) &= 1\,, && (S \text{ wave})\\ P^{(1)}_{\mu\mu'}(a) &= -g_{\mu\mu'} + \frac{p_{a,\mu}p_{a,\mu'}}{p_a^2}\,, && (P \text{ wave})\\ P^{(2)}_{\mu\nu\mu'\nu'}(a) &= \frac{1}{2}(P^{(1)}_{\mu\mu'}(a)P^{(1)}_{\nu\nu'}(a) + P^{(1)}_{\mu\nu'}(a)P^{(1)}_{\nu\mu'}(a)) - \frac{1}{3}P^{(1)}_{\mu\nu}(a)P^{(1)}_{\mu'\nu'}(a)\,. && (D \text{ wave})\end{aligned} \tag{4.16}$$

The pure orbital angular-momentum covariant tensors are given by

$$\begin{aligned}\tilde{t}^{(0)}_{\mu}(a) &= 1\,, && (S \text{ wave})\\ \tilde{t}^{(1)}_{\mu}(a) &= -P^{(1)}_{\mu\mu'}(a)r_a^{\mu'}\,, && (P \text{ wave})\\ \tilde{t}^{(2)}_{\mu\nu}(a) &= P^{(2)}_{\mu\nu\mu'\nu'}(a)r_a^{\mu'}r_a^{\nu'}\,, && (D \text{ wave})\end{aligned} \tag{4.17}$$

JHEP05(2025)195

Decay chain	$S(p)$
$D^+[S] \to V_1V_2$	$P^{(1)\mu\nu}(D^+)\tilde{t}^{(1)\mu}(V_1)\ \tilde{t}^{(1)}_{\nu}(V_2)$
$D^+[P] \to V_1V_2$	$\epsilon_{\mu\nu\lambda\sigma}p^{\mu}(D^+)\ \tilde{T}^{(1)\nu}(D^+)\tilde{t}^{(1)\lambda}(V_1)\ \tilde{t}^{(1)\sigma}(V_2)$
$D^+[D] \to V_1V_2$	$\tilde{T}^{(2)\mu\nu}(D^+)\tilde{t}^{(1)}_{\mu}(V_1)\ \tilde{t}^{(1)}_{\nu}(V_2)$
$D^+ \to AP_1, A[S] \to VP_2$	$\tilde{T}^{(1)\mu}(D^+)\ P^{(1)}_{\mu\nu}(A)\ \tilde{t}^{(1)\nu}(V)$
$D^+ \to AP_1, A[D] \to VP_2$	$\tilde{T}^{(1)\mu}(D^+)\ \tilde{t}^{(2)}_{\mu\nu}(A)\ \tilde{t}^{(1)\nu}(V)$
$D^+ \to V_1P_1, V_1 \to V_2P_2$	$\epsilon_{\mu\nu\lambda\sigma}p^{\mu}_{V1}r^{\nu}_{V1}p^{\lambda}_{P1}r^{\sigma}_{V2}$
$D^+ \to PP_1, P \to VP_2$	$p^{\mu}(P_2)\tilde{t}^{(1)}_{\mu}(V)$
$D^+ \to SV$	$\tilde{T}^{(1)\mu}(D^+)\ \tilde{t}^{(1)}_{\mu}(V)$
$D^+ \to TP, T \to VP$	$\tilde{T}^{(2)}_{\alpha\beta}(D^+)P^{(2)\alpha\beta\rho\mu}(T)\epsilon_{\mu\nu\lambda\sigma}\tilde{t}^{(2)\nu}_{\rho}(T)\ p^{\lambda}_{T}P^{(1)\sigma\delta}(T)\tilde{t}^{(1)}_{\delta}(V)$

Table 2. The spin factors $S(p)$ for the various contributions in the amplitude model. All operators, i.e. $\tilde{t}$ and $\tilde{T}$, have the same definitions as in ref. [43]. Scalar, pseudo-scalar, vector and axial-vector states are denoted by S, P, V and A, respectively. The $[S]$, $[P]$ and $[D]$ denote the orbital angular-momentum quantum numbers $L = 0, 1$ and 2, respectively.

where $r_a = p_b - p_c$. The spin factors $S(p)$ for the various components used in the analysis are listed in table 2. The tensor describing the D^+ decays with orbital angular-momentum quantum number l is denoted by $\tilde{T}^{(l)\mu}$ and that of the intermediate $a \to bc$ decay is denoted by $\tilde{t}^{(l)\mu}$, and the $\tilde{T}^{(l)\mu}$ has the same definition as $\tilde{t}^{(l)\mu}$ in ref. [43].

4.3 Fit results

Using the method described in section 4.2, we perform the fit in steps by adding resonances one by one. The statistical significance of the newly added resonance is calculated by considering the change in the log likelihood value and taking into account the change in the number of degrees of freedom.

The data-fitting process commences with a base model incorporating the amplitudes of $D^+ \to \bar{K}^*(892)^0\rho(770)^+$ and $D^+ \to \bar{K}_1(1400)^0\pi^+$ ($\bar{K}_1(1400)^0 \to \bar{K}^*(892)\pi$), as they are clearly observed in the corresponding invariant-mass spectra. The amplitude of $\bar{K}_1(1400)^0 \to \bar{K}^*(892)\pi$ is a combination of the amplitudes of $\bar{K}^*(892)^-\pi^+$ and $\bar{K}^*(892)^0\pi^0$, taking into account the Clebsch-Gordan (CG) relation, which is detailed in appendix B. The amplitudes $\bar{K}(1460)^0 \to \bar{K}^*(892)\pi$ and $\bar{K}^*(1680)^0 \to \bar{K}^*(892)\pi$ are also subject to the same relation.

The amplitudes $D^+ \to \bar{K}_1(1270)^0\pi^+$ ($\bar{K}_1(1270)^0 \to K^-\rho(770)^+$), $D^+ \to \bar{K}(1460)^0\pi^+$ ($\bar{K}(1460)^0 \to \bar{K}^*(892)\pi$), and $D^+ \to \bar{K}^*(1680)^0\pi^+$ ($\bar{K}^*(1680)^0 \to \bar{K}^*(892)\pi$) are added and the change in the fit quality is assessed. As $D^+ \to (K^-\pi^+)_{S-\text{wave}}\rho(770)^+$ and other non-resonant decay modes exhibit significances exceeding 5σ and help improving the fit quality, they are also included in the model. A comprehensive list of the other allowed contributions (based on known states) with statistical significances less than 5σ is provided in appendix C.

The fit fraction (FF) for the n^{th} amplitude is computed numerically with generator-level MC events with a definition

$$\text{FF}_n = \frac{\sum^{N_{\text{gen}}} \left|\rho_n e^{i\phi_n}\mathcal{A}_n\right|^2}{\sum^{N_{\text{gen}}} |\mathcal{M}|^2}, \tag{4.18}$$

JHEP05(2025)195

where $N_{\rm gen}$ is the number of PHSP MC events at generator level. The sum of these FFs may not be unity if there is net constructive or destructive interference. Interference (IN) between the $n^{\rm th}$ and $n'^{\rm th}$ amplitudes is defined as

$$\mathrm{IN}_{nn'} = \frac{\sum^{N_{\rm gen}} 2Re[\rho_n e^{i\phi_n}\mathcal{A}_n(\rho_{n'}e^{i\phi_{n'}}\mathcal{A}_{n'})^*]}{\sum^{N_{\rm gen}}|\mathcal{M}|^2}\,. \tag{4.19}$$

Here, the Re in the numerator takes the modulus of that component. The interferences between the amplitudes are listed in table 10 of appendix D.

In order to determine the statistical uncertainties of FFs, the amplitude coefficients are randomly sampled according to the covariant matrix. Then a Gaussian function is used to fit the distribution of each FF. The width of this function is assigned as the uncertainty of the corresponding FF.

The phases, FFs, and statistical significances for different amplitudes are listed in table 3. The projections of the data sample and the fit result on the invariant masses and the angular distributions are shown in figure 3. Here, the angle between the K^- and the D^+ in the $K^-\pi^+$ rest frame is denoted as θ_K, the angle between the π^+ and the D^+ direction in the $\pi^+\pi^0$ rest frame is referred as θ_π, and the angle between the normals of the decay planes defined in the D^+ rest frame by the $K^-\pi^+$ pair and the $\pi^+\pi^0$ pair is represented as θ_χ.

Then a "mixed-sample method" [49] has also been programed to check the goodness-of-fit of our fit result. According to the method, we can calculate the "T" value of the data and the fit result is determined to be 0.50, the corresponding p value is 0.3974, which indicates good fit quality.

4.4 Systematic uncertainties for the amplitude analysis

The systematic uncertainties for the amplitude analysis are described below and summarized in table 4.

I Amplitude model.
The masses and widths of resonances are adjusted by their corresponding uncertainties [6, 45]. The GS lineshape of $\rho(770)^+$ is replaced with the RBW formula. The coupling constants of the $K\pi$ S-wave model are varied within their uncertainties given in ref. [47]. The changes of the phases and FFs are assigned as the associated systematic uncertainties.

II Effective radius.
The associated systematic uncertainties are estimated by repeating the fit procedure by varying the effective radii of the barrier, R_r, of the intermediate states and D^+ mesons by $R_r/\sqrt{12} \approx 1\,\mathrm{GeV}^{-1}$.

III Background.
The background is determined from the inclusive MC sample, and the uncertainty from background is estimated by varying the $w_{\rm bkg}$ parameter in eq. (4.1) within $\pm1\sigma$ of its statistical uncertainty.

JHEP05(2025)195

Amplitude	Phase (rad)	FFs (%)	Significance (σ)
$D^+[S] \to \bar{K}^*(892)^0\rho(770)^+$	0.0(fixed)	66.5 ± 1.1 ± 3.0	$> 10\sigma$
$D^+[P] \to \bar{K}^*(892)^0\rho(770)^+$	1.45 ± 0.04 ± 0.08	1.9 ± 0.2 ± 0.2	$> 10\sigma$
$D^+ \to \bar{K}^*(892)^0\rho(770)^+$	–	68.4 ± 1.1 ± 2.6	$> 10\sigma$
$D^+ \to \bar{K}_1(1270)^0[S]\pi^+$, $\bar{K}_1(1270)^0 \to K^-\rho(770)^+$	-0.09 ± 0.03 ± 0.03	3.8 ± 0.3 ± 0.3	$> 10\sigma$
$D^+ \to \bar{K}_1(1400)^0[S]\pi^+$	0.40 ± 0.02 ± 0.04	7.5 ± 0.2 ± 0.3	$> 10\sigma$
$D^+ \to \bar{K}_1(1400)^0[D]\pi^+$	-2.42± 0.04 ± 0.04	0.5 ± 0.1 ± 0.1	$> 10\sigma$
$D^+ \to \bar{K}_1(1400)^0\pi^+$, $\bar{K}_1(1400)^0 \to \bar{K}^*(892)\pi$	–	7.3 ± 0.2 ± 0.3	$> 10\sigma$
$D^+ \to \bar{K}(1460)^0\pi^+$, $\bar{K}(1460)^0 \to \bar{K}^*(892)\pi$	0.41 ± 0.04 ± 0.07	5.1 ± 0.2 ± 0.3	$> 10\sigma$
$D^+ \to \bar{K}^*(1680)^0\pi^+$, $\bar{K}^*(1680)^0 \to \bar{K}^*(892)\pi$	1.13 ± 0.04 ± 0.09	3.8 ± 0.4 ± 0.8	$> 10\sigma$
$D^+ \to (K^-\pi^+)_{S-\text{wave}}\rho(770)^+$	2.90 ± 0.02 ± 0.04	18.3 ± 0.7 ± 0.7	$> 10\sigma$
$D^+ \to \bar{K}(1460)^0\pi^+$, $\bar{K}(1460)^0 \to K^-[\pi^+\pi^0]^{L=1}\pi$	-1.29 ± 0.08 ± 0.06	8.6 ± 0.8 ± 0.5	$> 10\sigma$
$D^+ \to \bar{K}(1460)^0\pi^+$, $\bar{K}(1460)^0 \to [K^-\pi]^{L=1}\pi$	-2.31 ± 0.07 ± 0.06	3.4 ± 0.5 ± 0.3	$> 10\sigma$
$D^+ \to [K^-\rho(770)^+]^{L=1}\pi^+$	-1.27 ± 0.04 ± 0.03	1.8 ± 0.1 ± 0.1	$> 10\sigma$
$D^+ \to [\bar{K}^*(892)\pi]^{L=1}\pi^+$	-2.63 ± 0.05 ± 0.06	0.8 ± 0.1 ± 0.1	$> 10\sigma$
$D^+ \to [\bar{K}^*(892)^0\pi^+]^{L=1}\pi^0$	-1.97 ± 0.05 ± 0.04	0.8 ± 0.2 ± 0.4	$> 10\sigma$
$D^+ \to [K^-[\pi^+\pi^0]^{L=1}]^{L=0}\pi^+$	-1.12 ± 0.08 ± 0.13	0.8 ± 0.2 ± 0.2	$> 10\sigma$
$D^+[S] \to [K^-\pi^+]^{L=1}\rho(770)^+$	-1.87 ± 0.12 ± 0.11	0.5 ± 0.1 ± 0.1	9.3σ

Table 3. Phases, FFs, and statistical significances for different amplitudes in $D^+ \to K^-\pi^+\pi^+\pi^0$. Groups of related amplitudes are separated by horizontal lines and the last row of each group gives the total fit fraction of the above components with interferences considered. The first and second uncertainties for the phases and FFs are statistical and systematic, respectively. The letters in bracket represent relative orbital angular momentum between resonances. The subscripts of S-wave denotes the S-wave that modeled by the LASS parameterization [48]. The decay of $\bar{K}^*(892)$ includes both $K^*(892)^-$ and $\bar{K}^*(892)^0$, taking into account Clebsch-Gordan relations (refer to appendix B).

IV Simulation effects.

To estimate the uncertainties associated with γ_ϵ, as defined in eq. (4.5), the amplitude model is refitted by varying PID, tracking and π^0 reconstruction efficiencies according to their uncertainties.

V Fit bias.

The uncertainty associated with the fit procedure is evaluated by studying signal MC samples. An ensemble of 600 signal MC samples are generated according to the results of the amplitude analysis to check the pull distribution. The pull variables, $\frac{V_{\text{fit}}-V_{\text{input}}}{\sigma_{\text{fit}}}$, are defined to evaluate the corresponding uncertainty, where V_{input} is the input value in the generator, and V_{fit} and σ_{fit} are the fit value and statistical uncertainty, respectively. The distribution of pull values for the 600 samples generated and fitted is expected to

JHEP05(2025)195

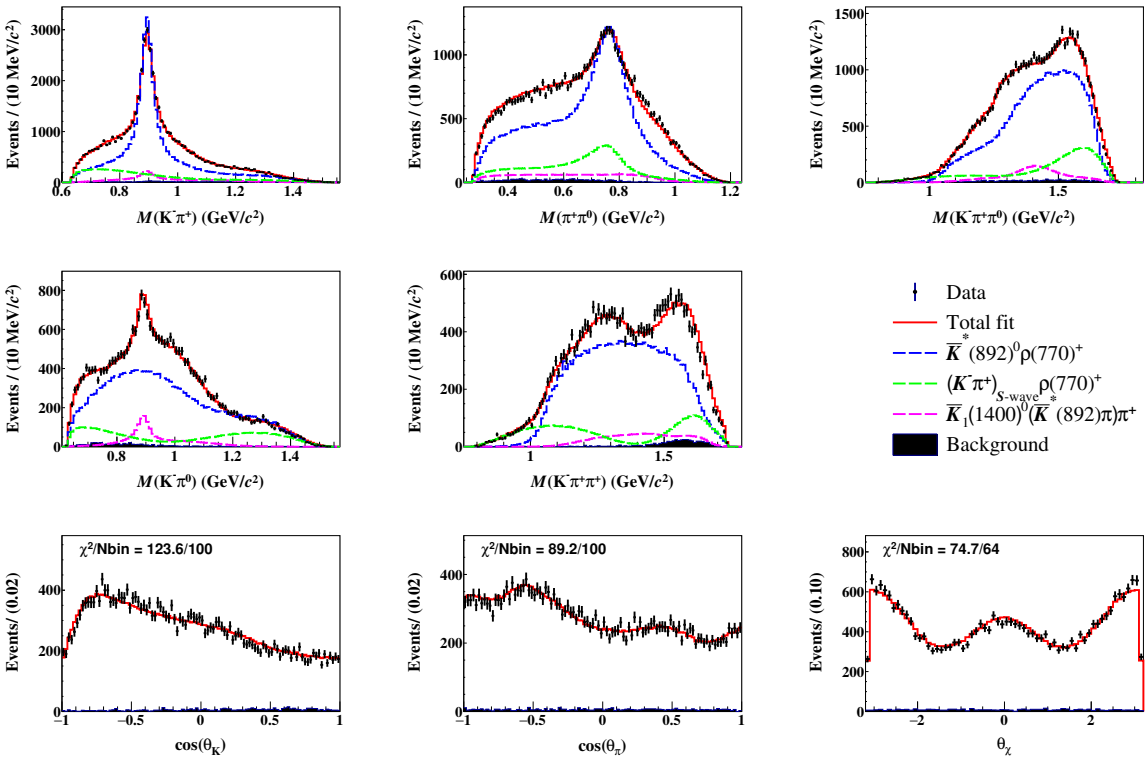

Figure 3. Projections of the data sample and the fit result on the invariant masses and the angular distributions. The data are represented by points with error bars, the fit results by the colored lines, and the background by black histogram. The combinations of two identical π^+ are added due to the exchange symmetry.

be a normal Gaussian distribution, and the uncertainty of the fitted mean values are assigned as the corresponding systematic uncertainties.

VI Insignificant amplitudes.

To achieve more reliable estimate of the model systematic effects, we have check the impact of the intermediate processes with statistical significances less than 5σ (Detailed in appendix C.) on the FF of the dominate process $D^+ \to \bar{K}^*(892)^0\rho(770)^+$. The model including $D^+ \to \pi^0\bar{K}_1(1400)^+, \bar{K}_1(1400)^+[D] \to \bar{K}^*(892)^0\pi^+$ has the largest variation with the nominal fit. Then the variation of the phases and FFs from the nominal result is taken as the corresponding systematic uncertainty.

5 Measurement of the branching fraction

The BF of $D^+ \to K^-\pi^+\pi^+\pi^0$ is measured with the DT technique using the same tag modes and event selection criteria as those described in section 3.

For a given ST mode, we have

$$N^{\rm ST}_{\rm tag} = 2N_{D^+D^-} \cdot \mathcal{B}_{\rm tag} \cdot \epsilon^{\rm ST}_{\rm tag}\,, \tag{5.1}$$

$$N^{\rm DT}_{\rm tag,sig} = 2N_{D^+D^-} \cdot \mathcal{B}_{\pi^0\to\gamma\gamma} \cdot \mathcal{B}_{\rm tag} \cdot \mathcal{B}_{\rm sig} \cdot \epsilon^{\rm DT}_{\rm tag,sig}\,, \tag{5.2}$$

JHEP05(2025)195

		Source						
Amplitude		I	II	III	IV	V	VI	Total
$D^+[S] \to \bar{K}^*(892)^0\rho(770)^+$	FF	0.50	0.31	0.08	0.05	0.06	2.65	2.72
$D^+[P] \to \bar{K}^*(892)^0\rho(770)^+$	ϕ	1.70	0.34	0.11	0.08	0.06	0.95	1.98
	FF	0.84	0.10	0.01	0.03	0.05	0.20	0.87
$D^+ \to \bar{K}^*(892)^0\rho(770)^+$	FF	0.48	0.26	0.07	0.04	0.04	2.33	2.40
$D^+ \to \bar{K}_1(1270)^0\pi^+$,	ϕ	0.90	0.22	0.04	0.09	0.05	0.22	0.96
$\bar{K}_1(1270)^0[S] \to K^-\rho(770)^+$	FF	0.31	0.15	0.10	0.15	0.06	0.95	1.03
$D^+ \to \bar{K}_1(1400)^0\pi^+$,	ϕ	1.80	0.33	0.03	0.01	0.06	0.70	1.96
$\bar{K}_1(1400)^0[S] \to \bar{K}^*(892)\pi$	FF	1.02	0.15	0.01	0.01	0.06	0.85	1.34
$D^+ \to \bar{K}_1(1400)^0\pi^+$,	ϕ	1.06	0.24	0.07	0.03	0.05	0.07	1.09
$\bar{K}_1(1400)^0[D] \to \bar{K}^*(892)\pi$	FF	0.20	0.10	0.10	0.01	0.05	0.01	0.25
$D^+ \to \bar{K}_1(1400)^0\pi^+$	FF	0.96	0.20	0.05	0.05	0.06	0.80	1.27
$D^+ \to \bar{K}(1460)^0\pi^+$,	ϕ	1.55	0.05	0.17	0.03	0.05	0.66	1.70
$\bar{K}(1460)^0 \to \bar{K}^*(892)\pi$	FF	1.49	0.30	0.15	0.01	0.05	0.35	1.57
$D^+ \to \bar{K}^*(1680)^0\pi^+$,	ϕ	2.19	0.21	0.02	0.01	0.06	0.14	2.20
$\bar{K}^*(1680)^0 \to \bar{K}^*(892)\pi$	FF	1.89	0.43	0.03	0.11	0.06	0.05	1.94
$D^+ \to (K^-\pi^+)_{S-\text{wave}}\rho(770)^+$	ϕ	1.76	0.52	0.06	0.04	0.06	0.38	1.88
	FF	0.95	0.15	0.03	0.08	0.06	0.15	0.98
$D^+ \to \bar{K}(1460)^0\pi^+$,	ϕ	0.42	0.26	0.01	0.05	0.06	0.52	0.72
$\bar{K}(1460)^0 \to K^-[\pi^+\pi^0]^{L=1}$	FF	0.51	0.03	0.02	0.14	0.06	0.32	0.62
$D^+ \to \bar{K}(1460)^0\pi^+$,	ϕ	0.76	0.37	0.03	0.06	0.06	0.14	0.86
$\bar{K}(1460)^0 \to [K^-\pi]^{L=1}\pi$	FF	0.34	0.60	0.02	0.04	0.06	0.56	0.89
$D^+ \to [K^-\rho(770)^+]^{L=1}\pi^+$	ϕ	0.43	0.53	0.04	0.05	0.04	0.31	0.75
	FF	0.47	0.70	0.01	0.20	0.05	0.40	0.96
$D^+ \to [\bar{K}^*(892)\pi]^{L=1}\pi^+$	ϕ	1.20	0.05	0.08	0.10	0.06	0.24	1.23
	FF	0.72	0.20	0.01	0.01	0.06	0.30	0.80
$D^+ \to [\bar{K}^*(892)^0\pi^+)]^{L=1}\pi^0$	ϕ	0.78	0.15	0.05	0.10	0.06	0.29	0.86
	FF	0.96	0.30	0.10	0.10	0.05	1.95	2.20
$D^+ \to [K^-[\pi^+\pi^-]^{L=1}]^{L=1}\pi^+$	ϕ	1.39	0.75	0.04	0.12	0.06	0.26	1.61
	FF	0.74	0.20	0.01	0.10	0.06	0.50	0.92
$D^+[S] \to [K^-\pi^+]^{L=1}\rho(770)^+$	ϕ	0.69	0.42	0.08	0.01	0.06	0.43	0.92
	FF	0.47	0.20	0.10	0.01	0.05	0.60	0.80

Table 4. Systematic uncertainties on the phases and FFs for the different components in the amplitude model in units of the corresponding statistical uncertainties. (I) Amplitude model, (II) Effective radius, (III) Background, (IV) Simulation effects, (V) Fit bias, and (VI) Insignificant amplitudes.

JHEP05(2025)195

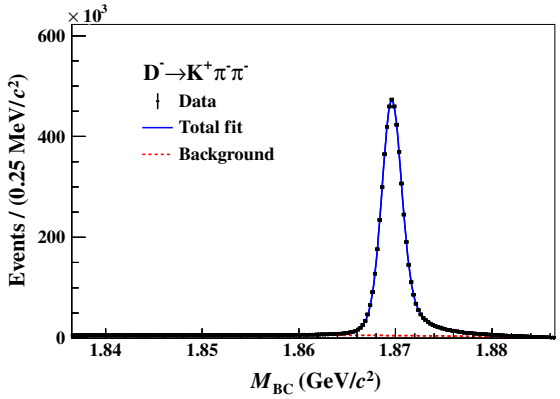

Figure 4. Fit to the $M_{\rm BC}$ distribution of the ST candidates.

Tag mode	ΔE (MeV)	$N^{\rm ST}_{\rm tag}$	$\epsilon^{\rm ST}_{\rm tag}(\%)$	$N^{\rm DT}_{\rm tag,sig}$	$\epsilon^{\rm DT}_{\rm tag,sig}(\%)$
$D^- \to K^+\pi^-\pi^-$	$[-25, 24]$	2215326 ± 1589	52.44 ± 0.01	35481 ± 220	14.03 ± 0.01

Table 5. The energy difference requirements, ST yields ($N^{\rm ST}_{\rm tag}$), ST efficiency ($\epsilon^{\rm ST}_{\rm tag}$), DT yields ($N^{\rm DT}_{\rm tag,sig}$) and DT efficiency ($\epsilon^{\rm DT}_{\rm tag,sig}$). The uncertainties are statistical only.

where $N^{\rm ST}_{\rm tag}$ is the ST yield for a specific tag mode, $N_{D^+D^-}$ is the total number of D^+D^- pairs produced from e^+e^- collisions, $\mathcal{B}_{\rm tag}$ and $\epsilon^{\rm ST}_{\rm tag}$ are the BF and the ST efficiency for tag mode, $N^{\rm DT}_{\rm tag,sig}$ is the DT yield, $\mathcal{B}_{\rm sig}$ and $\epsilon^{\rm DT}_{\rm tag,sig}$ are the BF of the signal mode and the efficiency for simultaneously reconstructing the signal and tag modes, $\mathcal{B}_{\pi^0\to\gamma\gamma}$ is the BF of $\pi^0 \to \gamma\gamma$ obtained from PDG [6]. Combining the two equations above, the absolute BF of $D^+ \to K^-\pi^+\pi^+\pi^0$ is

$$\mathcal{B}_{\rm sig} = \frac{N^{\rm DT}_{\rm tag,sig}}{\mathcal{B}_{\pi^0\to\gamma\gamma} \cdot N^{\rm ST}_{\rm tag} \cdot \epsilon^{\rm DT}_{\rm tag,sig}/\epsilon^{\rm ST}_{\rm tag}} . \tag{5.3}$$

The value of $N^{\rm ST}_{\rm tag}$ is obtained from a one-dimensional binned fit to the $M_{\rm BC}$ distribution, as shown in figure 4. The signal shape is modeled by the MC-simulated shape convolved with a double-Gaussian function describing the resolution difference between data and MC simulation, and the background shape is described by the ARGUS function [50]. The corresponding $\epsilon^{\rm ST}_{\rm tag}$ is estimated with the inclusive MC sample.

The DT yield is determined to be $N^{\rm DT}_{\rm tag,sig} = 35481 \pm 220$ through a fit to the $M_{\rm BC}$ distribution, as depicted in figure 5. Here, the signal shape is modeled by the MC-simulated shape convolved with a double-Gaussian function, and the background shape is described by the ARGUS function [50]. There are some peaking backgrounds from the processes $D^+ \to K\pi e^+\nu_e$ and $D^+ \to K\pi\mu^+\nu_\mu$, and they are described by the MC-simulated shape, and the corresponding contributions are fixed to the estimation from the MC simulation in the fit. $\epsilon^{\rm DT}_{\rm tag,sig}$ is determined with the signal MC sample in which the $D^+ \to K^-\pi^+\pi^+\pi^0$ events are generated according to the result of the amplitude analysis. The values of these parameters are summarized in table 5.

The systematic uncertainties for the branching fraction measurement are described below and summarized in table 6.

JHEP05(2025)195

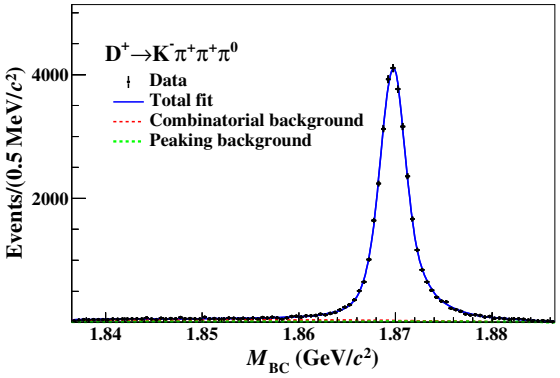

Figure 5. Fit to the $M_{\rm BC}$ distribution of the DT candidates.

- ST D^- candidates:

  the uncertainty in the yield of ST D mesons is assigned to be 0.1% from studies that involve varying the signal shape, background shape, and floating the parameters of the Gaussian in the fit [51].

- Tracking and PID:

  the tracking and PID efficiencies of $\pi^\pm$ and $K^\pm$ are investigated with DT hadronic $D\bar{D}$ events of the decays $D^0 \to K^-\pi^+$, $K^-\pi^+\pi^0$, $K^-\pi^+\pi^+\pi^-$ versus $\bar{D}^0 \to K^+\pi^-$, $K^+\pi^-\pi^0$, $K^+\pi^-\pi^-\pi^+$, and $D^+ \to K^-\pi^+\pi^+$ versus $D^- \to K^+\pi^-\pi^-$. The data-MC efficiency ratios for π and K tracking (PID) are found to be 0.996 ± 0.002 and 0.994 ± 0.003 (0.998 ± 0.001 and 0.998 ± 0.003). After correcting the MC efficiencies to data by these factors, the statistical uncertainties of the correction parameters are assigned as the systematic uncertainties. These are 0.4% and 0.3% (0.2% and 0.3%) for the π and K tracking (PID), respectively.

- π^0 reconstruction:

  the data-MC efficiency ratio for π^0 reconstruction is 0.974 ± 0.001, which is measured with samples of $D^0 \to K^-\pi^+\pi^0$ versus $\bar{D}^0 \to K^+\pi^-, K^+\pi^-\pi^0, K^+\pi^-\pi^-\pi^+$ hadronic decays. After correcting the efficiency of π^0 reconstruction by this factor, the associated systematic uncertainty is assigned as 0.1%.

- MC sample size:

  the statistical uncertainty arising from the limited size of the MC sample is 0.1%.

- Amplitude model:

  the uncertainty associated with the amplitude model is estimated by varying the fitted parameters based on the covariance matrix. The masses and widths of the intermediate resonances and R_r values are randomized according to a Gaussian distribution. The distribution of 300 efficiencies arising from this procedure is fitted by a Gaussian and the deviation from the nominal mean value, 0.8%, is taken as the systematic uncertainty.

JHEP05(2025)195

Source	Uncertainty (%)
ST D^- candidates	0.1
Tracking	0.7
PID	0.5
π^0 reconstruction	0.1
MC sample size	0.1
Amplitude model	0.8
$\mathcal{B}(\pi^0 \to \gamma\gamma)$	Negligible
Fit procedure	0.1
Total	1.2

Table 6. Relative systematic uncertainties in the BF measurement.

- The assumed BF:

  the BF of $\pi^0 \to \gamma\gamma$ is well known [6], and the uncertainty on this quantity induces a negligible uncertainty in the analysis.

- Fit procedure:

  the signal MC accurately describes the distribution in data, and the fit model includes a convolution of a free Gaussian function to account for residual discrepancies in data-MC resolution. Therefore, the primary source of systematic uncertainty in the fit procedure stems from the knowledge of the background shape. The uncertainty is estimated by shifting the end-point of the ARGUS function by $\pm 0.2\,\text{MeV}$, and varying the fixed value for the peaking background within a range of $\pm 1\sigma$ of its statistical uncertainty. The largest deviation in the measured BF, which is 0.1%, is assigned as the corresponding systematic uncertainty.

After correcting for the differences in π^+ tracking, PID and π^0 reconstruction efficiencies between data and MC simulation, the BF of $D^+ \to K^-\pi^+\pi^+\pi^0$ is determined to be $\mathcal{B}(D^+ \to K^-\pi^+\pi^+\pi^0) = (6.35 \pm 0.04_{\text{stat.}} \pm 0.07_{\text{syst.}})\%$.

6 Summary

An amplitude analysis of the Cabibbo-favoured decay $D^+ \to K^-\pi^+\pi^+\pi^0$ has been performed using 7.93 fb^{-1} of e^+e^- collision data collected with the BESIII detector at the center-of-mass energy of 3.773 GeV. With a detection efficiency based on the results of the amplitude analysis, we obtain $\mathcal{B}(D^+ \to K^-\pi^+\pi^+\pi^0) = (6.35 \pm 0.04_{\text{stat.}} \pm 0.07_{\text{syst.}})\%$. The result is consistent with the value of $\mathcal{B}(D^+ \to K^-\pi^+\pi^+\pi^0) = (5.98 \pm 0.08_{\text{stat.}} \pm 0.16_{\text{syst.}})\%$ measured by the CLEO collaboration [5]. Combining the FFs listed in table 3, the BFs for the intermediate processes are calculated with $\mathcal{B}_i = FF_i \times \mathcal{B}(D^+ \to K^-\pi^+\pi^+\pi^0)$, and the obtained results are listed in table 7.

According to the amplitude analysis, the dominant intermediate process is $D^+ \to \bar{K}^*(892)^0\rho(770)^+ \to K^-\pi^+\pi^+\pi^0$, with a BF of $(4.35 \pm 0.07_{\text{stat.}} \pm 0.17_{\text{syst.}})\%$. After applying

JHEP05(2025)195

Intermediate process	BF (10^{-2})
$D^+ \to \bar{K}^*(892)^0\rho(770)^+, \bar{K}^*(892)^0 \to K^-\pi^+, \rho(770)^+ \to \pi^+\pi^0$	$4.35 \pm 0.07 \pm 0.17$
$D^+ \to \bar{K}_1(1270)^0\pi^+, \bar{K}_1(1270)^0 \to K^-\rho(770)^+, \rho(770)^+ \to \pi^+\pi^0$	$0.24 \pm 0.02 \pm 0.02$
$D^+ \to \bar{K}_1(1400)^0\pi^+, \bar{K}_1(1400)^0 \to \bar{K}^*(892)\pi, \bar{K}^*(892) \to K\pi$	$0.46 \pm 0.01 \pm 0.02$
$D^+ \to \bar{K}(1460)^0\pi^+, \bar{K}(1460)^0 \to \bar{K}^*(892)\pi, \bar{K}^*(892) \to K\pi$	$0.32 \pm 0.01 \pm 0.02$
$D^+ \to \bar{K}(1680)^{*0}\pi^+, \bar{K}(1680)^{*0} \to \bar{K}^*(892)\pi, \bar{K}^*(892) \to K\pi$	$0.25 \pm 0.02 \pm 0.05$
$D^+ \to (K^-\pi^+)_{S-\text{wave}}\rho(770)^+, \rho(770)^+ \to \pi^+\pi^0$	$1.16 \pm 0.04 \pm 0.05$
$D^+ \to \bar{K}(1460)^0\pi^+, \bar{K}(1460)^0 \to K^-(\pi^+\pi^0)_V$	$0.53 \pm 0.05 \pm 0.03$
$D^+ \to \bar{K}(1460)^0\pi^+, \bar{K}(1460)^0 \to (K^-\pi)_V\pi$	$0.22 \pm 0.03 \pm 0.02$
$D^+ \to (K^-\rho(770)^+)_A\pi^+, \rho(770)^+ \to \pi^+\pi^0$	$0.11 \pm 0.01 \pm 0.01$
$D^+ \to (\bar{K}^*(892)\pi)_A\pi^+, \bar{K}^*(892) \to K\pi$	$0.05 \pm 0.01 \pm 0.01$
$D^+ \to (\bar{K}^*(892)^0\pi^+)_A\pi^0, \bar{K}^*(892)^0 \to K^-\pi^+$	$0.05 \pm 0.01 \pm 0.02$
$D^+ \to (K^-\pi^+)_V\rho(770)^+, \rho(770)^+ \to \pi^+\pi^0$	$0.03 \pm 0.01 \pm 0.01$
$D^+ \to (K^-(\pi^+\pi^0)_V)_P\pi^+$	$0.05 \pm 0.01 \pm 0.01$

Table 7. The BFs of various intermediate processes in $D^+ \to K^-\pi^+\pi^+\pi^0$. The first and second uncertainties are statistical and systematic, respectively.

Decay channel and Collaboration	$\mathcal{B}(D^+ \to \bar{K}^*(892)^0\rho(770)^+)$ ($\times 10^{-2}$)
$D^+ \to K^-\pi^+\pi^+\pi^0$, current analysis	$6.52 \pm 0.11 \pm 0.26$
$D^+ \to K^-\pi^+\pi^+\pi^0$, MARK-III [4]	$7.2 \pm 1.8 \pm 2.1$
$D^+ \to K^0_S\pi^+\pi^0\pi^0$, BESIII [21]	$5.82 \pm 0.49 \pm 0.29$

Table 8. Comparison of the BFs of the intermediate processes $D^+ \to \bar{K}^*(892)^0\rho(770)^+$ in the D hadronic decay. The first and second uncertainties are statistical and systematic, respectively.

the isospin symmetry assumption to the decays of $\bar{K}^*(892)^0 \to K^-\pi^+$ and $\bar{K}^*(892)^0 \to \bar{K}^0\pi^0$, the absolute BF of $D^+ \to \bar{K}^*(892)^0\rho(770)^+$ is determined to be $(6.52 \pm 0.11_{\text{stat.}} \pm 0.25_{\text{syst.}})\%$. As can be seen from table 8, this result is consistent with previous measurements from MARK-III [4] and BESIII [21], but is a factor of 10.1 and 2.1 times more precise, respectively.

The measured BF of $D^+ \to \bar{K}_1(1400)^0\pi^+$ is consistent with the previous BESIII result [21] within 1.5σ, but the precision is improved by a factor of 4.4. Information about the two K_1 states in this decay also provides inputs to further investigations of the mixing of the axial-vector kaon mesons [22, 23].

Acknowledgments

The BESIII Collaboration thanks the staff of BEPCII and the IHEP computing center for their strong support. This work is supported in part by National Key R&D Program of China under Contracts Nos. 2023YFA1606000, 2020YFA0406300, 2020YFA0406400; National Natural Science Foundation of China (NSFC) under Contracts Nos. 12375070, 11635010, 11735014, 11935015, 11935016, 11935018, 12025502, 12035009, 12035013, 12061131003, 12192260, 12192261, 12192262, 12192263, 12192264, 12192265, 12221005, 12225509, 12235017,

JHEP05(2025)195

12361141819; the Chinese Academy of Sciences (CAS) Large-Scale Scientific Facility Program; the CAS Center for Excellence in Particle Physics (CCEPP); Joint Large-Scale Scientific Facility Funds of the NSFC and CAS under Contract No. U1832207, U2032104; Shanghai Leading Talent Program of Eastern Talent Plan under Contract No. JLH5913002; the Excellent Youth Foundation of Henan Scientific Committee under Contract No. 242300421044; 100 Talents Program of CAS; The Institute of Nuclear and Particle Physics (INPAC) and Shanghai Key Laboratory for Particle Physics and Cosmology; German Research Foundation DFG under Contracts Nos. FOR5327, GRK 2149; Istituto Nazionale di Fisica Nucleare, Italy; Knut and Alice Wallenberg Foundation under Contracts Nos. 2021.0174, 2021.0299; Ministry of Development of Turkey under Contract No. DPT2006K-120470; National Research Foundation of Korea under Contract No. NRF-2022R1A2C1092335; National Science and Technology fund of Mongolia; National Science Research and Innovation Fund (NSRF) via the Program Management Unit for Human Resources & Institutional Development, Research and Innovation of Thailand under Contracts Nos. B16F640076, B50G670107; Polish National Science Centre under Contract No. 2019/35/O/ST2/02907; Swedish Research Council under Contract No. 2019.04595; The Swedish Foundation for International Cooperation in Research and Higher Education under Contract No. CH2018-7756; U. S. Department of Energy under Contract No. DE-FG02-05ER41374.

A $M_{\rm BC}^{\rm sig}$ versus $M_{\rm BC}^{\rm tag}$ two-dimensional fit

The signal yields of DT candidates are determined by a two-dimensional (2D) maximum likelihood bin fit to the distribution of $M_{\rm BC}^{\rm sig}$ versus $M_{\rm BC}^{\rm tag}$. Signal events with both and signal sides reconstructed correctly concentrate around $M_{\rm BC}^{\rm sig} = M_{\rm BC}^{\rm tag} = M_D$, where M_D is the known D mass [6]. We define three kinds of background. Candidates with correctly reconstructed D^+ (or D^-) and incorrectly reconstructed D^- (or D^+) are BKGI, which appear around the lines $M_{\rm BC}^{\rm sig}$ or $M_{\rm BC}^{\rm tag} = M_D$. Other candidates appearing around the diagonal are mainly from the $D^0\bar{D}^0$ mispartition and the $e^+e^- \to q\bar{q}$ processes (BKGII). The remaining combinatorial backgrounds mainly come from candidates reconstructed incorrectly on both sides (BKGIII). The PDFs for the different components used in the fit are given below:

- **Signal:** $\mathbf{s}(x, y)$**,**
- **BKGI:** $b_1(x) \cdot \mathcal{A}\mathbf{rgus}(y; m_0, c, p) + b_2(y) \cdot \mathcal{A}\mathbf{rgus}(x; m_0, c, p)$**,**
- **BKGII:** $\mathcal{A}\mathbf{gus}((x+y)/\sqrt{2}; m_0, c, p) \cdot g((x-y)/\sqrt{2})$**,**
- **BKGIII:** $\mathcal{A}\mathbf{rgus}(x; m_0, c, p) \cdot \mathcal{A}\mathbf{rgus}(y; m_0, c, p)$**.**

The signal shape $\mathrm{s}(x, y)$ is described by the 2D MC-simulated shape convolved with a 2D Gaussian. The parameters of the Gaussian function are obtained by one-dimensional (1D) fit on $M_{\rm BC}$ in signal and tag sides respectively, and are fixed in 2D fit. For BKGI, $b_{1,2}(x, y)$ is described by the 1D MC-simulated shape convolved with a Gaussian function, $\mathcal{A}\mathrm{rgus}(x, y)$ is the ARGUS function [50]. For BKGII, it is described by an ARGUS function in the diagonal axis multiplied by a Gaussian function in the anti-diagonal axis. For BKGIII, it constructed by an ARGUS function [50] in $M_{\rm BC}^{\rm sig}$ multiplied by an ARGUS function in $M_{\rm BC}^{\rm tag}$.

JHEP05(2025)195

Index	Amplitude	Relation
A_1	$D^+ \to \bar{K}_1(1400)^0\pi^+$, $\bar{K}_1(1400)^0 \to \bar{K}^*(892)^0\pi^0, \bar{K}^*(892)^0 \to K^-\pi^+$	
A_2	$D^+ \to \bar{K}_1(1400)^0\pi^+$, $\bar{K}_1(1400)^0 \to K^*(892)^-\pi^+, K^*(892)^- \to K^-\pi^0$	
A	$D^+ \to \bar{K}_1(1400)^0\pi^+$, $\bar{K}_1(1400)^0 \to K^*(892)\pi, K^*(892) \to K\pi$	$A_1 - A_2$
A_1	$D^+ \to \bar{K}(1460)^0\pi^+$, $\bar{K}(1460)^0 \to \bar{K}^*(892)^0\pi^0, \bar{K}^*(892)^0 \to K^-\pi^+$	
A_2	$D^+ \to \bar{K}(1460)^0\pi^+$, $\bar{K}(1460)^0 \to K^*(892)^-\pi^+, K^*(892)^- \to K^-\pi^0$	
A	$D^+ \to \bar{K}(1460)^0\pi^+$, $\bar{K}(1460)^0 \to K^*(892)\pi, K^*(892) \to K\pi$	$A_1 - A_2$
A_1	$D^+ \to \bar{K}^*(1680)^0\pi^+$, $\bar{K}^*(1680)^0 \to \bar{K}^*(892)^0\pi^0, \bar{K}^*(892)^0 \to K^-\pi^+$	
A_2	$D^+ \to \bar{K}^*(1680)^0\pi^+$, $\bar{K}^*(1680)^0 \to K^*(892)^-\pi^+, K^*(892)^- \to K^-\pi^0$	
A	$D^+ \to \bar{K}^*(1680)^0\pi^+$, $\bar{K}^*(1680)^0 \to K^*(892)\pi, K^*(892) \to K\pi$	$A_1 - A_2$

Table 9. The CG relations assumed in the analysis.

In the fit, the parameters m_0 and p for the ARGUS function [50] is fixed at $1.8865\,\mathrm{GeV}/c^2$ and 0.5, respectively.

B Clebsch-Gordan relations

Considering the isospin relationship in hadron decays, some amplitudes are fixed by CG relations, as listed in table 9. The amplitudes with fixed relations share the same magnitude (ρ) and phase (ϕ).

C Other intermediate processes tested

In this section, we list the significance and interference of the other possible combinations of the extra intermediate resonances that are considered in the amplitude analysis. Note that, the parameterized $\bar{K}^*(700)^0$ with T-matrix Pole (POLE) function as the propagator is labeled as $\bar{K}^*(700)^0$(POLE), and the parameterized $\bar{K}^*(700)^0$ with relativistic Breit-Wigner (RBW) function as the propagator is labeled as $\bar{K}^*(700)^0$(RBW).

- **Cascade amplitudes**

- $D^+[D] \to \bar{K}^*(892)^0\rho(770)^+$ (2.6σ),
- $D^+[S] \to \bar{K}^*(892)^0\rho(1450)^+$ (4.4σ),
- $D^+[P] \to \bar{K}^*(892)^0\rho(1450)^+$ (3.8σ),
- $D^+[D] \to \bar{K}^*(892)^0\rho(1450)^+$ (3.5σ),
- $D^+ \to \bar{K}^*(700)^0$(RBW)$\rho(770)^+(3.0\sigma)$,
- $D^+ \to \bar{K}^*(700)^0$(RBW)$\rho(1450)^+$ (1.5σ),
- $D^+ \to \bar{K}^*(700)^0$(POLE)$\rho(770)^+$ (3.0σ),
- $D^+ \to \bar{K}^*(700)^0$(POLE)$\rho(1450)^+$ (1.5σ),
- $D^+ \to \pi^+\bar{K}_1(1270)^0, \bar{K}_1(1270)^0[D] \to K^-\rho(770)^+$ (3.3σ),

JHEP05(2025)195

- $D^+ \to \pi^+ \bar{K}_1(1270)^0, \bar{K}_1(1270)^0[S] \to \bar{K}^*\pi$ ($<1\sigma$),
- $D^+ \to \pi^+ \bar{K}_1(1270)^0, \bar{K}_1(1270)^0[D] \to \bar{K}^*\pi$ ($<1\sigma$),
- $D^+ \to \pi^0 \bar{K}_1(1270)^+, \bar{K}_1(1270)^+[S] \to \bar{K}^*(892)^0\pi^+$ ($<1\sigma$),
- $D^+ \to \pi^0 \bar{K}_1(1270)^+, \bar{K}_1(1270)^+[D] \to \bar{K}^*(892)^0\pi^+$ (3.1σ),
- $D^+ \to \pi^+ \bar{K}_1(1400)^0, \bar{K}_1(1400)^0[S] \to K^-\rho(770)^+$ (2.3σ),
- $D^+ \to \pi^+ \bar{K}_1(1400)^0, \bar{K}_1(1400)^0[D] \to K^-\rho(770)^+$ (1.6σ),
- $D^+ \to \pi^0 \bar{K}_1(1400)^+, \bar{K}_1(1400)^+[S] \to \bar{K}^*(892)^0\pi^+$ (3.9σ),
- $D^+ \to \pi^0 \bar{K}_1(1400)^+, \bar{K}_1(1400)^+[D] \to \bar{K}^*(892)^0\pi^+$ (4.5σ),
- $D^+ \to \bar{K}^*(1410)^0\pi^+, \bar{K}^*(1410)^0 \to \bar{K}^*\pi$ (1.9σ),
- $D^+ \to \bar{K}^*(1410)^0\pi^+, \bar{K}^*(1410)^0 \to K^-\rho(770)^+$ (1.3σ),
- $D^+ \to \bar{K}^*(1410)^0\pi^+, \bar{K}^*(1410)^0 \to \bar{K}^*(892)^0\pi^+$ ($<1\sigma$),
- $D^+ \to \pi^+ \bar{K}(1460)^0, \bar{K}(1460)^0 \to K^-\rho(770)^+$ (4.7σ),
- $D^+ \to \pi^+ \bar{K}_1(1650)^0, \bar{K}_1(1650)^0[S, D] \to K^*(892)\pi$ (3.0σ),
- $D^+ \to \bar{K}^*(1680)^0\pi^+, \bar{K}^*(1680)^0 \to K^-\rho(770)^+$ (4.5σ),
- $D^+ \to \bar{K}^*(1680)^+\pi^0, \bar{K}^*(1680)^+ \to \bar{K}^*(892)^0\pi^+$ (2.3σ).
- $D^+ \to \bar{K}_2^*(1430)^0\pi^+, \bar{K}_2^*(1430)^0 \to \bar{K}^*(892)\pi$ (1.6σ).
- $D^+ \to \bar{K}_2^*(1430)^+\pi^0, \bar{K}_2^*(1430)^+ \to \bar{K}^*(892)^0\pi^+$ (2.1σ).
- $D^+ \to \bar{K}_2(1580)^0\pi^0, \bar{K}_2^(1580)^0 \to \bar{K}^*(892)\pi$ (1.4σ).
- $D^+ \to \bar{K}_2(1580)^+\pi^0, \bar{K}_2^(1580)^+ \to \bar{K}^*(892)^0\pi^+$ (1.8σ).

- **Three-body amplitudes**

- $D^+[S] \to \bar{K}^*(892)^0(\pi^+\pi^0)_V$ (2.4σ),
- $D^+[P] \to \bar{K}^*(892)^0(\pi^+\pi^0)_V$ (2.1σ),
- $D^+[D] \to \bar{K}^*(892)^0(\pi^+\pi^0)_V$ (1.6σ),
- $D^+[P] \to \rho(770)^+(K^-\pi^+)_V$ (4.3σ),
- $D^+[D] \to \rho(770)^+(K^-\pi^+)_V$ (2.3σ),
- $D^+[S] \to \rho(1450)^+(K^-\pi^+)_V$ (2.6σ),
- $D^+[P] \to \rho(1450)^+(K^-\pi^+)_V$ (2.4σ),
- $D^+[D] \to \rho(1450)^+(K^-\pi^+)_V$ (2.0σ),
- $D^+ \to \rho(770)^+(K^-\pi^+)_{S-\text{wave}}$ (2.0σ),
- $D^+ \to \bar{K}^*(700)^0(\text{RBW})(\pi^+\pi^0)_V$ (3.0σ),
- $D^+ \to \bar{K}^*(700)^0(\text{RBW})(\pi^+\pi^0)_S$ (1.2σ),
- $D^+ \to \bar{K}^*(700)^0(\text{POLE})(\pi^+\pi^0)_V$ (2.7σ),
- $D^+ \to \bar{K}^*(700)^0(\text{POLE})(\pi^+\pi^0)_S$ (0.9σ).

JHEP05(2025)195

- **Four-body non-resonance amplitudes**

- $D^+ \to (K^-((\pi^+\pi^0)_{S-\text{wave}})_A\pi^+)$ $(< 1\sigma)$,
- $D^+ \to (K^-((\pi^+\pi^0)_{S-\text{wave}})_P\pi^+)$ (1.6σ),
- $D^+ \to (K^-((\pi^+\pi^0)_{S-\text{wave}})_V\pi^+)$ $(< 1\sigma)$,
- $D^+ \to \pi^0((K^-\pi^+)_{S-\text{wave}}\pi^+)_A$ $(< 1\sigma)$,
- $D^+ \to \pi^0((K^-\pi^+)_{S-\text{wave}}\pi^+)_P$ $(< 1\sigma)$,
- $D^+ \to \pi^+((K^-\pi^+)_{S-\text{wave}}\pi^+)_V$ (2.3σ),
- $D^+ \to \pi^+((K^-\pi^+)_V\pi^0)_A$ $(< 1\sigma)$,
- $D^+ \to \pi^+((K^-\pi^+)_V\pi^0)_P$ $(< 1\sigma)$,
- $D^+ \to \pi^+((K^-\pi^+)_V\pi^0)_V$ $(< 1\sigma)$,
- $D^+ \to (K^-\pi^+\pi^+\pi^0)_{\text{non-resonance}}$ (3.2σ).

D The interference between processes

The interference between processes calculated by Equation (4.19).

I $D^+[S] \to \bar{K}^*(892)^0\rho(770)^+$,

II $D^+[P] \to \bar{K}^*(892)^0\rho(770)^+$,

III $D^+ \to \bar{K}_1(1270)^0\pi^+[S]$,

IV $D^+ \to \bar{K}_1(1400)^0\pi^+[S]$,

V $D^+ \to \bar{K}_1(1400)^0\pi^+[D]$,

VI $D^+ \to \bar{K}(1460)^0\pi^+$,

VII $D^+ \to \bar{K}^*(1680)^0\pi^+$,

VIII $D^+ \to (K^-\pi^+)_{S-\text{wave}}\rho(770)^+$,

IX $D^+ \to \bar{K}(1460)^0\pi^+$, $\bar{K}(1460)^0 \to K^-(\pi^+\pi^0)_V$,

X $D^+ \to \bar{K}(1460)^0\pi^+$, $\bar{K}(1460)^0 \to (K^-\pi)_V\pi$,

XI $D^+ \to (K^-\rho(770)^+)_A\pi^+$,

XII $D^+ \to (\bar{K}^*(892)\pi)_A\pi^+$,

XIII $D^+ \to (\bar{K}^*(892)^0\pi^+)_A\pi^0$,

XIV $D^+ \to (K^-(\pi^+\pi^-)_V)_P\pi^+$,

XV $D^+[S] \to (K^-\pi^+)_V\rho(770)^+$.

JHEP05(2025)195

	II	III	IV	V	VI	VII	VIII	IX	X	XI	XII	XIII	XIV	XV
– I	−0.02	4.72	−6.74	3.76	−5.36	3.85	−4.23	2.19	4.54	−2.06	−8.12	−4.19	8.42	−0.76
II		0.00	0.00	0.00	0.00	−0.87	0.87	0.00	0.01	0.01	0.00	0.00	0.00	0.00
III			−2.89	2.84	−0.13	0.18	2.89	−3.19	0.25	−0.40	−0.49	0.63	0.26	−0.65
IV				−1.44	−0.96	2.40	−2.18	2.10	1.30	3.43	8.61	−4.11	−2.61	0.68
V					0.07	−0.07	0.56	−0.58	0.03	−0.06	0.35	−0.26	0.01	−0.24
VI						0.00	0.03	2.21	−4.46	2.63	−0.36	1.31	−0.79	−0.60
VII							−0.01	0.02	0.2	0.01	0.00	0.00	0.00	0.00
VIII								3.26	−10.26	6.52	−1.63	3.04	6.66	−6.56
IX									−5.84	6.37	−0.14	0.29	3.02	−2.45
X										−0.74	0.87	1.11	−3.74	3.09
XI											−0.44	0.25	0.45	0.03
XII												1.14	−1.02	0.30
XIII													0.67	−0.33
XIV														0.15

Table 10. Interference of each amplitude, in unit of % of total amplitude.

Data Availability Statement. This article has no associated data or the data will not be deposited.

Code Availability Statement. This article has no associated code or the code will not be deposited.

References

[1] BESIII collaboration, *Study of $D^+ \to K^-\pi^+e^+\nu_e$*, *Phys. Rev. D* **94** (2016) 032001 [arXiv:1512.08627] [INSPIRE].

[2] BESIII collaboration, *Observation of the Semileptonic D^+ Decay into the $\bar{K}_1(1270)^0$ Axial-Vector Meson*, *Phys. Rev. Lett.* **123** (2019) 231801 [arXiv:1907.11370] [INSPIRE].

[3] BESIII collaboration, *Observation of the Doubly Cabibbo-Suppressed Decay $D^+ \to K^+\pi^+\pi^-\pi^0$ and Evidence for $D^+ \to K^+\omega$*, *Phys. Rev. Lett.* **125** (2020) 141802 [arXiv:2007.07674] [INSPIRE].

[4] MARK-III collaboration, *Resonant substructure in $\bar{K}\pi\pi\pi$ decays of D mesons*, *Phys. Rev. D* **45** (1992) 2196 [INSPIRE].

[5] CLEO collaboration, *Measurement of absolute hadronic branching fractions of D mesons and $e^+e^- \to D\bar{D}$ cross-sections at the $\psi(3770)$*, *Phys. Rev. D* **76** (2007) 112001 [arXiv:0709.3783] [INSPIRE].

[6] Particle Data Group collaboration, *Review of Particle Physics*, *PTEP* **2022** (2022) 083C01 [INSPIRE].

JHEP05(2025)195

[7] H.J. Lipkin, *Puzzles in hyperon, charm and beauty physics*, *Nucl. Phys. B Proc. Suppl.* **115** (2003) 117 [hep-ph/0210166] [INSPIRE].

[8] H.-Y. Cheng and C.-W. Chiang, *Two-body hadronic charmed meson decays*, *Phys. Rev. D* **81** (2010) 074021 [arXiv:1001.0987] [INSPIRE].

[9] CLEO collaboration, *Measurement of exclusive D meson decays to η and η' final states and SU(3) amplitude analysis*, *Phys. Rev. D* **77** (2008) 092003 [arXiv:0802.2664] [INSPIRE].

[10] BESIII collaboration, *Dalitz Plot Analysis of the Decay $\omega \to \pi^+\pi^-\pi^0$*, *Phys. Rev. D* **98** (2018) 112007 [arXiv:1811.03817] [INSPIRE].

[11] FOCUS collaboration, *Dalitz plot analysis of the $D^+ \to K^-\pi^+\pi^+$ decay in the FOCUS experiment*, *Phys. Lett. B* **653** (2007) 1 [arXiv:0705.2248] [INSPIRE].

[12] BESIII collaboration, *Amplitude Analysis of the $D^+ \to K^0_S\pi^+\pi^0$ Dalitz Plot*, *Phys. Rev. D* **89** (2014) 052001 [arXiv:1401.3083] [INSPIRE].

[13] BESIII collaboration, *Study of the decay $D^+ \to K^*(892)^+K^0_S$ in $D^+ \to K^+K^0_S\pi^0$*, *Phys. Rev. D* **104** (2021) 012006 [arXiv:2104.09131] [INSPIRE].

[14] M. Bauer, B. Stech and M. Wirbel, *Exclusive Nonleptonic Decays of D, D_s, and B-Mesons*, *Z. Phys. C* **34** (1987) 103 [INSPIRE].

[15] A.N. Kamal, R.C. Verma and N. Sinha, *$(D, D^+_s \to VV)$ decays in two models: an SU(3)-symmetry model and a factorization model with final-state interactions*, *Phys. Rev. D* **43** (1991) 843 [INSPIRE].

[16] I. Hinchliffe and T.A. Kaeding, *Nonleptonic two-body decays of D mesons in broken SU(3)*, *Phys. Rev. D* **54** (1996) 914 [hep-ph/9502275] [INSPIRE].

[17] E.H.E. Aaoud and A.N. Kamal, *Helicity and partial wave amplitude analysis of $D \to K^*\rho$ decay*, *Phys. Rev. D* **59** (1999) 114013 [hep-ph/9910350] [INSPIRE].

[18] X.-W. Kang and H.-B. Li, *Study of CP violation in $D \to VV$ decay at BESIII*, *Phys. Lett. B* **684** (2010) 137 [arXiv:0912.3068] [INSPIRE].

[19] Y. Cao, Y. Cheng and Q. Zhao, *Resolving the polarization puzzles in $D^0 \to VV$*, *Phys. Rev. D* **109** (2024) 073002 [arXiv:2303.00535] [INSPIRE].

[20] BESIII collaboration, *Amplitude analysis and branching fraction measurement of the decay $D^+_s \to K^+\pi^+\pi^-\pi^0$*, *JHEP* **09** (2022) 242 [arXiv:2205.13759] [INSPIRE].

[21] BESIII collaboration, *Amplitude analysis and branching fraction measurement of the decay $D^+ \to K^0_S\pi^+\pi^0\pi^0$*, *JHEP* **09** (2023) 077 [arXiv:2305.15879] [INSPIRE].

[22] H.-Y. Cheng, *Revisiting Axial-Vector Meson Mixing*, *Phys. Lett. B* **707** (2012) 116 [arXiv:1110.2249] [INSPIRE].

[23] P.-F. Guo, D. Wang and F.-S. Yu, *Strange Axial-vector Mesons in D Meson Decays*, *Nucl. Phys. Rev.* **36** (2019) 125 [arXiv:1801.09582] [INSPIRE].

[24] BESIII collaboration, *Measurement of the integrated luminosities of the data taken by BESIII at $\sqrt{s} = 3.650$ and 3.773 GeV*, *Chin. Phys. C* **37** (2013) 123001 [arXiv:1307.2022] [INSPIRE].

[25] BESIII collaboration, *Measurement of integrated luminosity of data collected at 3.773 GeV by BESIII from 2021 to 2024*, *Chin. Phys. C* **48** (2024) 123001 [arXiv:2406.05827] [INSPIRE].

[26] BESIII collaboration, *Design and Construction of the BESIII Detector*, *Nucl. Instrum. Meth. A* **614** (2010) 345 [arXiv:0911.4960] [INSPIRE].

JHEP05(2025)195

[27] C. Yu et al., *BEPCII Performance and Beam Dynamics Studies on Luminosity*, in the proceedings of the *7th International Particle Accelerator Conference*, Busan, South Korea, May 08–13 (2016) [DOI:10.18429/JACoW-IPAC2016-TUYA01] [INSPIRE].

[28] BESIII collaboration, *Future Physics Programme of BESIII*, *Chin. Phys. C* **44** (2020) 040001 [arXiv:1912.05983] [INSPIRE].

[29] J. Lu, Y. Xiao and X. Ji, *Online monitoring of the center-of-mass energy from real data at BESIII*, *Radiat. Detect. Technol. Methods* **4** (2020) 337 [INSPIRE].

[30] J.-W. Zhang et al., *Suppression of top-up injection backgrounds with offline event filter in the BESIII experiment*, *Radiat. Detect. Technol. Methods* **6** (2022) 289 [INSPIRE].

[31] X. Li et al., *Study of MRPC technology for BESIII endcap-TOF upgrade*, *Radiat. Detect. Technol. Methods* **1** (2017) 13 [INSPIRE].

[32] Y.-X. Guo et al., *The study of time calibration for upgraded end cap TOF of BESIII*, *Radiat. Detect. Technol. Methods* **1** (2017) 15 [INSPIRE].

[33] P. Cao et al., *Design and construction of the new BESIII endcap Time-of-Flight system with MRPC Technology*, *Nucl. Instrum. Meth. A* **953** (2020) 163053 [INSPIRE].

[34] GEANT4 collaboration, *GEANT4 - A Simulation Toolkit*, *Nucl. Instrum. Meth. A* **506** (2003) 250 [INSPIRE].

[35] S. Jadach, B.F.L. Ward and Z. Was, *Coherent exclusive exponentiation for precision Monte Carlo calculations*, *Phys. Rev. D* **63** (2001) 113009 [hep-ph/0006359] [INSPIRE].

[36] S. Jadach, B.F.L. Ward and Z. Was, *The Precision Monte Carlo event generator KK for two fermion final states in e^+e^- collisions*, *Comput. Phys. Commun.* **130** (2000) 260 [hep-ph/9912214] [INSPIRE].

[37] D.J. Lange, *The EvtGen particle decay simulation package*, *Nucl. Instrum. Meth. A* **462** (2001) 152 [INSPIRE].

[38] R.-G. Ping, *Event generators at BESIII*, *Chin. Phys. C* **32** (2008) 599 [INSPIRE].

[39] J.C. Chen et al., *Event generator for J/ψ and $\psi(2S)$ decay*, *Phys. Rev. D* **62** (2000) 034003 [INSPIRE].

[40] R.-L. Yang, R.-G. Ping and H. Chen, *Tuning and Validation of the Lundcharm Model with J/ψ Decays*, *Chin. Phys. Lett.* **31** (2014) 061301 [INSPIRE].

[41] E. Barberio, B. van Eijk and Z. Was, *PHOTOS: a Universal Monte Carlo for QED radiative corrections in decays*, *Comput. Phys. Commun.* **66** (1991) 115 [INSPIRE].

[42] MARK-III collaboration, *Direct Measurements of Charmed d Meson Hadronic Branching Fractions*, *Phys. Rev. Lett.* **56** (1986) 2140 [INSPIRE].

[43] B.S. Zou and D.V. Bugg, *Covariant tensor formalism for partial-wave analyses of ψ decay to mesons*, *Eur. Phys. J. A* **16** (2003) 537 [hep-ph/0211457] [INSPIRE].

[44] BESIII collaboration, *Amplitude analysis and branching fraction measurement of $D_s^+ \to K^+K^-\pi^+$*, *Phys. Rev. D* **104** (2021) 012016 [arXiv:2011.08041] [INSPIRE].

[45] P. d'Argent et al., *Amplitude Analyses of $D^0 \to \pi^+\pi^-\pi^+\pi^-$ and $D^0 \to K^+K^-\pi^+\pi^-$ Decays*, *JHEP* **05** (2017) 143 [arXiv:1703.08505] [INSPIRE].

[46] G.J. Gounaris and J.J. Sakurai, *Finite width corrections to the vector meson dominance prediction for $\rho \to e^+e^-$*, *Phys. Rev. Lett.* **21** (1968) 244 [INSPIRE].

JHEP05(2025)195

[47] D. Aston et al., *A study of $K^-\pi^+$ scattering in the reaction $K^-p \to K^-\pi^+n$ at 11 GeV/c*, *Nucl. Phys. B* **296** (1988) 493 [INSPIRE].

[48] BABAR and BELLE collaborations, *Measurement of $\cos 2\beta$ in $B^0 \to D^{(*)}h^0$ with $D \to K^0_S\pi^+\pi^-$ decays by a combined time-dependent Dalitz plot analysis of BaBar and Belle data*, *Phys. Rev. D* **98** (2018) 112012 [arXiv:1804.06153] [INSPIRE].

[49] M. Williams, *How good are your fits? Unbinned multivariate goodness-of-fit tests in high energy physics*, 2010 *JINST* **5** P09004 [arXiv:1006.3019] [INSPIRE].

[50] ARGUS collaboration, *Search for Hadronic $b \to u$ Decays*, *Phys. Lett. B* **241** (1990) 278 [INSPIRE].

[51] BESIII collaboration, *Search for $D^0 \to K^0_S K^- e^+ \nu_e, D^+ \to K^0_S K^0_S e^+ \nu_e$, and $D^+ \to K^+ K^- e^+ \nu_e$*, *Phys. Rev. D* **109** (2024) 072003 [arXiv:2312.07572] [INSPIRE].

JHEP05(2025)195

The BESIII collaboration

M. Ablikim[1], M.N. Achasov[4,c], P. Adlarson[76], O. Afedulidis[3], X.C. Ai[81], R. Aliberti[35], A. Amoroso[75A,75C], Y. Bai[57], O. Bakina[36], I. Balossino[29A], Y. Ban[46,h], H.-R. Bao[64], V. Batozskaya[1,44], K. Begzsuren[32], N. Berger[35], M. Berlowski[44], M. Bertani[28A], D. Bettoni[29A], F. Bianchi[75A,75C], E. Bianco[75A,75C], A. Bortone[75A,75C], I. Boyko[36], R.A. Briere[5], A. Brueggemann[69], H. Cai[77], X. Cai[1,58], A. Calcaterra[28A], G.F. Cao[1,64], N. Cao[1,64], S.A. Cetin[62A], X.Y. Chai[46,h], J.F. Chang[1,58], G.R. Che[43], Y.Z. Che[1,58,64], G. Chelkov[36,b], C. Chen[43], C.H. Chen[9], Chao Chen[55], G. Chen[1], H.S. Chen[1,64], H.Y. Chen[20], M.L. Chen[1,58,64], S.J. Chen[42], S.L. Chen[45], S.M. Chen[61], T. Chen[1,64], X.R. Chen[31,64], X.T. Chen[1,64], Y.B. Chen[1,58], Y.Q. Chen[34], Z.J. Chen[25,i], S.K. Choi[10], G. Cibinetto[29A], F. Cossio[75C], J.J. Cui[50], H.L. Dai[1,58], J.P. Dai[79], A. Dbeyssi[18], R.E. de Boer[3], D. Dedovich[36], C.Q. Deng[73], Z.Y. Deng[1], A. Denig[35], I. Denysenko[36], M. Destefanis[75A,75C], F. De Mori[75A,75C], B. Ding[67,1], X.X. Ding[46,h], Y. Ding[40], Y. Ding[34], J. Dong[1,58], L.Y. Dong[1,64], M.Y. Dong[1,58,64], X. Dong[77], M.C. Du[1], S.X. Du[81], Y.Y. Duan[55], Z.H. Duan[42], P. Egorov[36,b], G.F. Fan[42], J.J. Fan[19], Y.H. Fan[45], J. Fang[1,58], J. Fang[59], S.S. Fang[1,64], W.X. Fang[1], Y. Fang[1], Y.Q. Fang[1,58], R. Farinelli[29A], L. Fava[75B,75C], F. Feldbauer[3], G. Felici[28A], C.Q. Feng[72,58], J.H. Feng[59], Y.T. Feng[72,58], M. Fritsch[3], C.D. Fu[1], J.L. Fu[64], Y.W. Fu[1,64], H. Gao[64], X.B. Gao[41], Y.N. Gao[19], Y.N. Gao[46,h], Yang Gao[72,58], S. Garbolino[75C], I. Garzia[29A,29B], P.T. Ge[19], Z.W. Ge[42], C. Geng[59], E.M. Gersabeck[68], A. Gilman[70], K. Goetzen[13], L. Gong[40], W.X. Gong[1,58], W. Gradl[35], S. Gramigna[29A,29B], M. Greco[75A,75C], M.H. Gu[1,58], Y.T. Gu[15], C.Y. Guan[1,64], A.Q. Guo[31,64], L.B. Guo[41], M.J. Guo[50], R.P. Guo[49], Y.P. Guo[12,g], A. Guskov[36,b], J. Gutierrez[27], K.L. Han[64], T.T. Han[1], F. Hanisch[3], X.Q. Hao[19], F.A. Harris[66], K.K. He[55], K.L. He[1,64], F.H. Heinsius[3], C.H. Heinz[35], Y.K. Heng[1,58,64], C. Herold[60], T. Holtmann[3], P.C. Hong[34], G.Y. Hou[1,64], X.T. Hou[1,64], Y.R. Hou[64], Z.L. Hou[1], B.Y. Hu[59], H.M. Hu[1,64], J.F. Hu[56,j], Q.P. Hu[72,58], S.L. Hu[12,g], T. Hu[1,58,64], Y. Hu[1], G.S. Huang[72,58], K.X. Huang[59], L.Q. Huang[31,64], P. Huang[42], X.T. Huang[50], Y.P. Huang[1], Y.S. Huang[59], T. Hussain[74], F. Hölzken[3], N. Hüsken[35], N. in der Wiesche[69], J. Jackson[27], S. Janchiv[32], Q. Ji[1], Q.P. Ji[19], W. Ji[1,64], X.B. Ji[1,64], X.L. Ji[1,58], Y.Y. Ji[50], X.Q. Jia[50], Z.K. Jia[72,58], D. Jiang[1,64], H.B. Jiang[77], P.C. Jiang[46,h], S.S. Jiang[39], T.J. Jiang[16], X.S. Jiang[1,58,64], Y. Jiang[64], J.B. Jiao[50], J.K. Jiao[34], Z. Jiao[23], S. Jin[42], Y. Jin[67], M.Q. Jing[1,64], X.M. Jing[64], T. Johansson[76], S. Kabana[33], N. Kalantar-Nayestanaki[65], X.L. Kang[9], X.S. Kang[40], M. Kavatsyuk[65], B.C. Ke[81], V. Khachatryan[27], A. Khoukaz[69], R. Kiuchi[1], O.B. Kolcu[62A], B. Kopf[3], M. Kuessner[3], X. Kui[1,64], N. Kumar[26], A. Kupsc[44,76], W. Kühn[37], W.N. Lan[19], T.T. Lei[72,58], Z.H. Lei[72,58], M. Lellmann[35], T. Lenz[35], C. Li[43], C. Li[47], C.H. Li[39], Cheng Li[72,58], D.M. Li[81], F. Li[1,58], G. Li[1], H.B. Li[1,64], H.J. Li[19], H.N. Li[56,j], Hui Li[43], J.R. Li[61], J.S. Li[59], K. Li[1], K.L. Li[19], L.J. Li[1,64], L.K. Li[1], Lei Li[48], M.H. Li[43], P.L. Li[64], P.R. Li[38,k,l], Q.M. Li[1,64], Q.X. Li[50], R. Li[17,31], T. Li[50], T.Y. Li[43], W.D. Li[1,64], W.G. Li[1,a], X. Li[1,64], X.H. Li[72,58], X.L. Li[50], X.Y. Li[1,8], X.Z. Li[59], Y. Li[19], Y.G. Li[46,h], Z.J. Li[59], Z.Y. Li[79], C. Liang[42], H. Liang[72,58], H. Liang[1,64], Y.F. Liang[54], Y.T. Liang[31,64], G.R. Liao[14], Y.P. Liao[1,64], J. Libby[26], A. Limphirat[60], C.C. Lin[55], C.X. Lin[64], D.X. Lin[31,64], T. Lin[1], B.J. Liu[1], B.X. Liu[77], C. Liu[34], C.X. Liu[1], F. Liu[1], F.H. Liu[53], Feng Liu[6], G.M. Liu[56,j], H. Liu[38,k,l], H.B. Liu[15], H.H. Liu[1], H.M. Liu[1,64], Huihui Liu[21], J.B. Liu[72,58], J.Y. Liu[1,64], K. Liu[38,k,l], K.Y. Liu[40], Ke Liu[22], L. Liu[72,58], L.C. Liu[43], Lu Liu[43], M.H. Liu[12,g], P.L. Liu[1], Q. Liu[64], S.B. Liu[72,58], T. Liu[12,g], W.K. Liu[43], W.M. Liu[72,58], X. Liu[39], X. Liu[38,k,l], Y. Liu[38,k,l], Y. Liu[81], Y.B. Liu[43], Z.A. Liu[1,58,64], Z.D. Liu[9], Z.Q. Liu[50], X.C. Lou[1,58,64], F.X. Lu[59], H.J. Lu[23], J.G. Lu[1,58], Y. Lu[7], Y.P. Lu[1,58], Z.H. Lu[1,64], C.L. Luo[41], J.R. Luo[59], M.X. Luo[80], T. Luo[12,g], X.L. Luo[1,58], X.R. Lyu[64], Y.F. Lyu[43],

JHEP05(2025)195

F.C. Ma[40], H. Ma[79], H.L. Ma[1], J.L. Ma[1,64], L.L. Ma[50], L.R. Ma[67], M.M. Ma[1,64], Q.M. Ma[1], R.Q. Ma[1,64], R.Y. Ma[19], T. Ma[72,58], X.T. Ma[1,64], X.Y. Ma[1,58], Y.M. Ma[31], F.E. Maas[18], I. MacKay[70], M. Maggiora[75A,75C], S. Malde[70], Y.J. Mao[46,h], Z.P. Mao[1], S. Marcello[75A,75C], Y.H. Meng[64], Z.X. Meng[67], J.G. Messchendorp[13,65], G. Mezzadri[29A], H. Miao[1,64], T.J. Min[42], R.E. Mitchell[27], X.H. Mo[1,58,64], B. Moses[27], N. Yu. Muchnoi[4,c], J. Muskalla[35], Y. Nefedov[36], F. Nerling[18,e], L.S. Nie[20], I.B. Nikolaev[4,c], Z. Ning[1,58], S. Nisar[11,m], Q.L. Niu[38,k,l], W.D. Niu[55], Y. Niu [50], S.L. Olsen[10,64], Q. Ouyang[1,58,64], S. Pacetti[28B,28C], X. Pan[55], Y. Pan[57], A. Pathak[10], Y.P. Pei[72,58], M. Pelizaeus[3], H.P. Peng[72,58], Y.Y. Peng[38,k,l], K. Peters[13,e], J.L. Ping[41], R.G. Ping[1,64], S. Plura[35], V. Prasad[33], F.Z. Qi[1], H. Qi[72,58], H.R. Qi[61], M. Qi[42], S. Qian[1,58], W.B. Qian[64], C.F. Qiao[64], J.H. Qiao[19], J.J. Qin[73], L.Q. Qin[14], L.Y. Qin[72,58], X.P. Qin[12,g], X.S. Qin[50], Z.H. Qin[1,58], J.F. Qiu[1], Z.H. Qu[73], C.F. Redmer[35], K.J. Ren[39], A. Rivetti[75C], M. Rolo[75C], G. Rong[1,64], Ch. Rosner[18], M.Q. Ruan[1,58], S.N. Ruan[43], N. Salone[44], A. Sarantsev[36,d], Y. Schelhaas[35], K. Schoenning[76], M. Scodeggio[29A], K.Y. Shan[12,g], W. Shan[24], X.Y. Shan[72,58], Z.J. Shang[38,k,l], J.F. Shangguan[16], L.G. Shao[1,64], M. Shao[72,58], C.P. Shen[12,g], H.F. Shen[1,8], W.H. Shen[64], X.Y. Shen[1,64], B.A. Shi[64], H. Shi[72,58], J.L. Shi[12,g], J.Y. Shi[1], S.Y. Shi[73], X. Shi[1,58], J.J. Song[19], T.Z. Song[59], W.M. Song[34,1], Y. J. Song[12,g], Y.X. Song[46,h,n], S. Sosio[75A,75C], S. Spataro[75A,75C], F. Stieler[35], S. S Su[40], Y.J. Su[64], G.B. Sun[77], G.X. Sun[1], H. Sun[64], H.K. Sun[1], J.F. Sun[19], K. Sun[61], L. Sun[77], S.S. Sun[1,64], T. Sun[51,f], Y.J. Sun[72,58], Y.Z. Sun[1], Z.Q. Sun[1,64], Z.T. Sun[50], C.J. Tang[54], G.Y. Tang[1], J. Tang[59], M. Tang[72,58], Y.A. Tang[77], L.Y. Tao[73], Q.T. Tao[25,i], M. Tat[70], J.X. Teng[72,58], V. Thoren[76], W.H. Tian[59], Y. Tian[31,64], Z.F. Tian[77], I. Uman[62B], Y. Wan[55], S.J. Wang[50], B. Wang[1], Bo Wang[72,58], C. Wang[19], D.Y. Wang[46,h], H.J. Wang[38,k,l], J.J. Wang[77], J.P. Wang [50], K. Wang[1,58], L.L. Wang[1], L.W. Wang[34], M. Wang[50], N.Y. Wang[64], S. Wang[12,g], S. Wang[38,k,l], T. Wang[12,g], T.J. Wang[43], W. Wang[59], W. Wang[73], W.P. Wang[35,58,72,o], X. Wang[46,h], X.F. Wang[38,k,l], X.J. Wang[39], X.L. Wang[12,g], X.N. Wang[1], Y. Wang[61], Y.D. Wang[45], Y.F. Wang[1,58,64], Y.H. Wang[38,k,l], Y.L. Wang[19], Y.N. Wang[45], Y.Q. Wang[1], Yaqian Wang[17], Yi Wang[61], Z. Wang[1,58], Z.L. Wang[73], Z.Y. Wang[1,64], D.H. Wei[14], F. Weidner[69], S.P. Wen[1], Y.R. Wen[39], U. Wiedner[3], G. Wilkinson[70], M. Wolke[76], L. Wollenberg[3], C. Wu[39], J.F. Wu[1,8], L.H. Wu[1], L.J. Wu[1,64], Lianjie Wu[19], X. Wu[12,g], X.H. Wu[34], Y.H. Wu[55], Y.J. Wu[31], Z. Wu[1,58], L. Xia[72,58], X.M. Xian[39], B.H. Xiang[1,64], T. Xiang[46,h], D. Xiao[38,k,l], G.Y. Xiao[42], H. Xiao[73], S.Y. Xiao[1], Y. L. Xiao[12,g], Z.J. Xiao[41], C. Xie[42], X.H. Xie[46,h], Y. Xie[50], Y.G. Xie[1,58], Y.H. Xie[6], Z.P. Xie[72,58], T.Y. Xing[1,64], C.F. Xu[1,64], C.J. Xu[59], G.F. Xu[1], M. Xu[72,58], Q.J. Xu[16], Q.N. Xu[30], W.L. Xu[67], X.P. Xu[55], Y. Xu[40], Y.C. Xu[78], Z.S. Xu[64], F. Yan[12,g], L. Yan[12,g], W.B. Yan[72,58], W.C. Yan[81], W.P. Yan[19], X.Q. Yan[1,64], H.J. Yang[51,f], H.L. Yang[34], H.X. Yang[1], J.H. Yang[42], R.J. Yang[19], T. Yang[1], Y. Yang[12,g], Y.F. Yang[43], Y.F. Yang[1,64], Y.X. Yang[1,64], Y.Z. Yang[19], Z.W. Yang[38,k,l], Z.P. Yao[50], M. Ye[1,58], M.H. Ye[8], J.H. Yin[1], Junhao Yin[43], Z.Y. You[59], B.X. Yu[1,58,64], C.X. Yu[43], G. Yu[1,64], J.S. Yu[25,i], M.C. Yu[40], T. Yu[73], X.D. Yu[46,h], C.Z. Yuan[1,64], J. Yuan[34], J. Yuan[45], L. Yuan[2], S.C. Yuan[1,64], Y. Yuan[1,64], Z.Y. Yuan[59], C.X. Yue[39], Ying Yue[19], A.A. Zafar[74], F.R. Zeng[50], S.H. Zeng[63], X. Zeng[12,g], Y. Zeng[25,i], Y.J. Zeng[59], Y.J. Zeng[1,64], X.Y. Zhai[34], Y.C. Zhai[50], Y.H. Zhan[59], A.Q. Zhang[1,64], B.L. Zhang[1,64], B.X. Zhang[1], D.H. Zhang[43], G.Y. Zhang[19], H. Zhang[81], H. Zhang[72,58], H.C. Zhang[1,58,64], H.H. Zhang[59], H.Q. Zhang[1,58,64], H.R. Zhang[72,58], H.Y. Zhang[1,58], J. Zhang[59], J. Zhang[81], J.J. Zhang[52], J.L. Zhang[20], J.Q. Zhang[41], J.S. Zhang[12,g], J.W. Zhang[1,58,64], J.X. Zhang[38,k,l], J.Y. Zhang[1], J.Z. Zhang[1,64], Jianyu Zhang[64], L.M. Zhang[61], Lei Zhang[42], P. Zhang[1,64], Q. Zhang[19], Q.Y. Zhang[34], R.Y. Zhang[38,k,l], S.H. Zhang[1,64], Shulei Zhang[25,i],

JHEP05(2025)195

X.M. Zhang[1], X. Y Zhang[40], X.Y. Zhang[50], Y. Zhang[73], Y. Zhang[1], Y. T. Zhang[81], Y.H. Zhang[1,58], Y.M. Zhang[39], Yan Zhang[72,58], Z.D. Zhang[1], Z.H. Zhang[1], Z.L. Zhang[34], Z.X. Zhang[19], Z.Y. Zhang[43], Z.Y. Zhang[77], Z.Z. Zhang[45], Zh. Zh. Zhang[19], G. Zhao[1], J.Y. Zhao[1,64], J.Z. Zhao[1,58], L. Zhao[1], Lei Zhao[72,58], M.G. Zhao[43], N. Zhao[79], R.P. Zhao[64], S.J. Zhao[81], Y.B. Zhao[1,58], Y.X. Zhao[31,64], Z.G. Zhao[72,58], A. Zhemchugov[36,b], B. Zheng[73], B.M. Zheng[34], J.P. Zheng[1,58], W.J. Zheng[1,64], X.R. Zheng[19], Y.H. Zheng[64], B. Zhong[41], X. Zhong[59], H. Zhou[35,50,o], J.Y. Zhou[34], L.P. Zhou[1,64], S. Zhou[6], X. Zhou[77], X.K. Zhou[6], X.R. Zhou[72,58], X.Y. Zhou[39], Y.Z. Zhou[12,g], Z.C. Zhou[20], A.N. Zhu[64], J. Zhu[43], K. Zhu[1], K.J. Zhu[1,58,64], K.S. Zhu[12,g], L. Zhu[34], L.X. Zhu[64], S.H. Zhu[71], T.J. Zhu[12,g], W.D. Zhu[41], W.Z. Zhu[19], Y.C. Zhu[72,58], Z.A. Zhu[1,64], J.H. Zou[1], J. Zu[72,58]

[1] *Institute of High Energy Physics, Beijing 100049, People's Republic of China*
[2] *Beihang University, Beijing 100191, People's Republic of China*
[3] *Bochum Ruhr-University, D-44780 Bochum, Germany*
[4] *Budker Institute of Nuclear Physics SB RAS (BINP), Novosibirsk 630090, Russia*
[5] *Carnegie Mellon University, Pittsburgh, Pennsylvania 15213, U.S.A.*
[6] *Central China Normal University, Wuhan 430079, People's Republic of China*
[7] *Central South University, Changsha 410083, People's Republic of China*
[8] *China Center of Advanced Science and Technology, Beijing 100190, People's Republic of China*
[9] *China University of Geosciences, Wuhan 430074, People's Republic of China*
[10] *Chung-Ang University, Seoul, 06974, Republic of Korea*
[11] *COMSATS University Islamabad, Lahore Campus, Defence Road, Off Raiwind Road, 54000 Lahore, Pakistan*
[12] *Fudan University, Shanghai 200433, People's Republic of China*
[13] *GSI Helmholtzcentre for Heavy Ion Research GmbH, D-64291 Darmstadt, Germany*
[14] *Guangxi Normal University, Guilin 541004, People's Republic of China*
[15] *Guangxi University, Nanning 530004, People's Republic of China*
[16] *Hangzhou Normal University, Hangzhou 310036, People's Republic of China*
[17] *Hebei University, Baoding 071002, People's Republic of China*
[18] *Helmholtz Institute Mainz, Staudinger Weg 18, D-55099 Mainz, Germany*
[19] *Henan Normal University, Xinxiang 453007, People's Republic of China*
[20] *Henan University, Kaifeng 475004, People's Republic of China*
[21] *Henan University of Science and Technology, Luoyang 471003, People's Republic of China*
[22] *Henan University of Technology, Zhengzhou 450001, People's Republic of China*
[23] *Huangshan College, Huangshan 245000, People's Republic of China*
[24] *Hunan Normal University, Changsha 410081, People's Republic of China*
[25] *Hunan University, Changsha 410082, People's Republic of China*
[26] *Indian Institute of Technology Madras, Chennai 600036, India*
[27] *Indiana University, Bloomington, Indiana 47405, U.S.A.*
[28] *INFN Laboratori Nazionali di Frascati , (A)INFN Laboratori Nazionali di Frascati, I-00044, Frascati, Italy; (B)INFN Sezione di Perugia, I-06100, Perugia, Italy; (C)University of Perugia, I-06100, Perugia, Italy*
[29] *INFN Sezione di Ferrara, (A)INFN Sezione di Ferrara, I-44122, Ferrara, Italy; (B)University of Ferrara, I-44122, Ferrara, Italy*
[30] *Inner Mongolia University, Hohhot 010021, People's Republic of China*
[31] *Institute of Modern Physics, Lanzhou 730000, People's Republic of China*
[32] *Institute of Physics and Technology, Peace Avenue 54B, Ulaanbaatar 13330, Mongolia*
[33] *Instituto de Alta Investigación, Universidad de Tarapacá, Casilla 7D, Arica 1000000, Chile*
[34] *Jilin University, Changchun 130012, People's Republic of China*
[35] *Johannes Gutenberg University of Mainz, Johann-Joachim-Becher-Weg 45, D-55099 Mainz, Germany*
[36] *Joint Institute for Nuclear Research, 141980 Dubna, Moscow region, Russia*
[37] *Justus-Liebig-Universitaet Giessen, II. Physikalisches Institut, Heinrich-Buff-Ring 16, D-35392 Giessen, Germany*

JHEP05(2025)195

[38] Lanzhou University, Lanzhou 730000, People's Republic of China
[39] Liaoning Normal University, Dalian 116029, People's Republic of China
[40] Liaoning University, Shenyang 110036, People's Republic of China
[41] Nanjing Normal University, Nanjing 210023, People's Republic of China
[42] Nanjing University, Nanjing 210093, People's Republic of China
[43] Nankai University, Tianjin 300071, People's Republic of China
[44] National Centre for Nuclear Research, Warsaw 02-093, Poland
[45] North China Electric Power University, Beijing 102206, People's Republic of China
[46] Peking University, Beijing 100871, People's Republic of China
[47] Qufu Normal University, Qufu 273165, People's Republic of China
[48] Renmin University of China, Beijing 100872, People's Republic of China
[49] Shandong Normal University, Jinan 250014, People's Republic of China
[50] Shandong University, Jinan 250100, People's Republic of China
[51] Shanghai Jiao Tong University, Shanghai 200240, People's Republic of China
[52] Shanxi Normal University, Linfen 041004, People's Republic of China
[53] Shanxi University, Taiyuan 030006, People's Republic of China
[54] Sichuan University, Chengdu 610064, People's Republic of China
[55] Soochow University, Suzhou 215006, People's Republic of China
[56] South China Normal University, Guangzhou 510006, People's Republic of China
[57] Southeast University, Nanjing 211100, People's Republic of China
[58] State Key Laboratory of Particle Detection and Electronics, Beijing 100049, Hefei 230026, People's Republic of China
[59] Sun Yat-Sen University, Guangzhou 510275, People's Republic of China
[60] Suranaree University of Technology, University Avenue 111, Nakhon Ratchasima 30000, Thailand
[61] Tsinghua University, Beijing 100084, People's Republic of China
[62] Turkish Accelerator Center Particle Factory Group, (A)Istinye University, 34010, Istanbul, Turkey; (B)Near East University, Nicosia, North Cyprus, 99138, Mersin 10, Turkey
[63] University of Bristol, H H Wills Physics Laboratory, Tyndall Avenue, Bristol, BS8 1TL, U.K.
[64] University of Chinese Academy of Sciences, Beijing 100049, People's Republic of China
[65] University of Groningen, NL-9747 AA Groningen, The Netherlands
[66] University of Hawaii, Honolulu, Hawaii 96822, U.S.A.
[67] University of Jinan, Jinan 250022, People's Republic of China
[68] University of Manchester, Oxford Road, Manchester, M13 9PL, United Kingdom
[69] University of Muenster, Wilhelm-Klemm-Strasse 9, 48149 Muenster, Germany
[70] University of Oxford, Keble Road, Oxford OX13RH, United Kingdom
[71] University of Science and Technology Liaoning, Anshan 114051, People's Republic of China
[72] University of Science and Technology of China, Hefei 230026, People's Republic of China
[73] University of South China, Hengyang 421001, People's Republic of China
[74] University of the Punjab, Lahore-54590, Pakistan
[75] University of Turin and INFN, (A)University of Turin, I-10125, Turin, Italy; (B)University of Eastern Piedmont, I-15121, Alessandria, Italy; (C)INFN, I-10125, Turin, Italy
[76] Uppsala University, Box 516, SE-75120 Uppsala, Sweden
[77] Wuhan University, Wuhan 430072, People's Republic of China
[78] Yantai University, Yantai 264005, People's Republic of China
[79] Yunnan University, Kunming 650500, People's Republic of China
[80] Zhejiang University, Hangzhou 310027, People's Republic of China
[81] Zhengzhou University, Zhengzhou 450001, People's Republic of China

[a] Deceased
[b] Also at the Moscow Institute of Physics and Technology, Moscow 141700, Russia
[c] Also at the Novosibirsk State University, Novosibirsk, 630090, Russia
[d] Also at the NRC "Kurchatov Institute", PNPI, 188300, Gatchina, Russia
[e] Also at Goethe University Frankfurt, 60323 Frankfurt am Main, Germany

JHEP05(2025)195

[f] Also at Key Laboratory for Particle Physics, Astrophysics and Cosmology, Ministry of Education; Shanghai Key Laboratory for Particle Physics and Cosmology; Institute of Nuclear and Particle Physics, Shanghai 200240, People's Republic of China
[g] Also at Key Laboratory of Nuclear Physics and Ion-beam Application (MOE) and Institute of Modern Physics, Fudan University, Shanghai 200443, People's Republic of China
[h] Also at State Key Laboratory of Nuclear Physics and Technology, Peking University, Beijing 100871, People's Republic of China
[i] Also at School of Physics and Electronics, Hunan University, Changsha 410082, China
[j] Also at Guangdong Provincial Key Laboratory of Nuclear Science, Institute of Quantum Matter, South China Normal University, Guangzhou 510006, China
[k] Also at MOE Frontiers Science Center for Rare Isotopes, Lanzhou University, Lanzhou 730000, People's Republic of China
[l] Also at Lanzhou Center for Theoretical Physics, Lanzhou University, Lanzhou 730000, People's Republic of China
[m] Also at the Department of Mathematical Sciences, IBA, Karachi 75270, Pakistan
[n] Also at Ecole Polytechnique Federale de Lausanne (EPFL), CH-1015 Lausanne, Switzerland
[o] Also at Helmholtz Institute Mainz, Staudinger Weg 18, D-55099 Mainz, Germany

JHEP05(2025)195